CONTROL OF A BIPEDAL HUMANOID ROBOT FOR TROLLEY PUSHING APPLICATIONS

by

CEM KAAN KARATAŞ

Submitted to the Graduate School of Engineering and Natural Sciences
in partial fulfillment of the requirements for the degree of Master of Science

Sabancı University

June 2024

ABSTRACT

CONTROL OF A BIPEDAL HUMANOID ROBOT FOR TROLLEY PUSHING APPLICATIONS

CEM KAAN KARATAŞ

MECHATRONICS ENGINEERING M.A. THESIS, JULY 2024

Thesis Supervisor: Assoc. Prof. Dr. Kemalettin Erbatur

Keywords: Humanoid Robot, Zero Moment Point, Linear Inverted Pendulum Model, Bipedal Walk, Full-Body Motion Control, Trolley Pushing

The state of art in humanoid robotics is gradually improving in the last 40 years. While the industrial robot became a standard production support tool within few decades after its introduction in 1950s, the development pace of human shaped counter parts towards an era of daily life human-robot coexistence is limited. This is primarily due to the challenges of the bipedal kinematic arrangement, balancing requirements, difficulties in its control and last, but not the least safety related problems.

Despite the drawbacks, the bipedal humanoid structure is popular because of its potential in operating in human environment, using tools and user interfaces meant for human personnel. A robot of with a humanoid kinematic arrangement can climb stairs, fit in a car and reach various instruments and appliances designed for human ergonomy. However, for the structure to be useful, the robot's skill level must match the advantages of the shape. A large class of physical work involves manipulation tasks through hands and walking or balancing on the feet. Such functions are treated in the framework of full-body motion control for humanoid robots.

Pushing a trolley is a common task in both industrial and everyday life circumstances. This thesis is centered on this motion. To this end, a combination of reference generation and control techniques are applied for the legs and arms of the humanoid. Walking reference trajectories are based on the Zero Moment Point Criterion. When hands are in contact with the trolley, a foot-ground interaction force planner enhances body posture control. Hands are subject to position control when not contacting and are controlled via hybrid position-force control when they push the trolley.

Reference generation and control system is tested on the dynamic simulation environment of the humanoid robot SURALP designed at Sabancı University.

ÖZET

EL ABARASI İTME UYGULAMALARI İÇİN İKİ AYAKLI INSANSI ROBOTUN KONTROLÜ

CEM KAAN KARATAŞ

MEKATRONİK MÜHENDİSLİĞİ YÜKSEK LİSANS TEZİ, ARALIK 2024

Tez Danışmanı: Doç Dr. Kemalettin Erbatur

Keywords:
Anahtar Kelimeler: İnsansı Robot, Sıfır Moment Noktası, Doğrusal Ters Sarkaç Modeli, İki Ayaklı Yürüyüş, Tüm Vücut Hareket Kontrolü, El arabası İtme

İnsansı robot bilimindeki son teknoloji son 40 yılda giderek gelişiyor. Endüstriyel robot, 1950'lerde piyasaya sürülmesinden sonraki birkaç on yıl içinde standart bir üretim destek aracı haline gelirken, insan şeklindeki karşı parçaların günlük yaşamda insan-robot bir arada yaşama çağına doğru gelişme hızı sınırlıdır. Bunun başlıca nedeni iki ayaklı kinematik düzenlemenin getirdiği zorluklar, dengeleme gereklilikleri, kontrolündeki zorluklar ve son olarak güvenlikle ilgili sorunlardır.

Dezavantajlarına rağmen iki ayaklı insansı yapı, insan ortamında çalışma, insan personele yönelik araçları ve kullanıcı arayüzlerini kullanma potansiyeli nedeniyle popülerdir. İnsansı kinematik düzenlemeye sahip bir robot, merdiven çıkabiliyor, bir arabaya sığabiliyor ve insan ergonomisine uygun olarak tasarlanmış çeşitli alet ve cihazlara ulaşabiliyor. Ancak yapının kullanışlı olması için robotun beceri düzeyinin yapının avantajlarıyla eşleşmesi gerekir. Fiziksel işlerin büyük bir çoğunluğu, eller aracılığıyla manipülasyon görevlerini ve ayakları üzerinde yürümeyi veya dengelemeyi içerir. Bu tür işlevler, insansı robotlar için tam vücut hareket kontrolü çerçevesinde ele alınır.

Bir arabayı itmek hem endüstriyel hem de günlük yaşam koşullarında yaygın bir iştir. Bu tez bu hareket üzerine yoğunlaşmıştır. Bu amaçla insansı robotun bacakları ve kolları için referans oluşturma ve kontrol tekniklerinin bir kombinasyonu uygulandı. Yürüme referans yörüngeleri Sıfır Moment Noktası Kriterini temel alır. Eller araba ile temas halindeyken, ayak-yer etkileşimi kuvvet planlayıcısı vücut duruşu kontrolünü geliştirir. Eller temas halinde değilken konum kontrolüne tabidir ve arabayı ittiklerinde hibrit konum-kuvvet kontrolü aracılığıyla kontrol edilir.

Referans oluşturma ve kontrol sistemi, Sabancı Üniversitesi'nde tasarlanan insansı robot SURALP'in dinamik simülasyon ortamında test edilmiştir.

TABLE OF CONTENTS

LIST OF TABLES

LIST OF FIGURES

1. INTRODUCTION

The humanoid robot researches have been steadily increasing in the last 40 years. Different countries, universites and companies have been investing money and resources. In 1960s Waseda University was one of the first institutes to develop their humanoid robot projects with WL,WABIAN and WABOT series. (Lim & Takanshi 2007) ASIMO was developed by HONDA with a goal to create a new form of mobility that could be of practical help to humans.(Hirose & Ogawa 2007) Beijing Institute of Technology (BIT) researched humanoid robots and their capabilities with their BHR series robots. (Huan et al. 2019) The Humanoid Robot Project (HRP) was established in 1998 by the Japanese Ministry of Economy and Industry. In collaboration with HONDA and AIST several humanoid robots were developed by this project. (Hirukuwa et al 2004) Boston Dynamics and their humanoid robot ATLAS has been popular in recent years due to the entertaining videos of ATLAS, moving really similar to a human. (Boson Dynamics, 2024)

While the research continues on humanoid robots, industrial robots became an essential part of the production lines allowing for a better efficiency. The difference between usage of humanoid and industrial robots lies within the challanges of bipedal kinematic arrangement, balancing requirments, difficulties in its control and safety related issues. It is easier to use an industrial robot which is mounted to a fixed point allowing for much easier control. Also, the level of human-robot interaction is lower with industrial robots which requires less safety precautions.

Despite the drawback the bipedal humanoid structure is widely used due to its easier integration to human environments. The potential of humanoid robots realizing tasks which are designed for human anatomy is crucial. However, the robot’s integration with its environments can be as good as its skill level. Hence, significant amount of research was conducted to make sure the robot can keep its balance while realizing different tasks.

First, a balance criterion needs to be defined to ensure the robot can stay on its feet. Zero Moment Point (ZMP) and Center of Mass(CoM) balance criterions are the most popular ones.(Shimmiyo et al. 2013)(Harada et al. 2013) Even with a proper balancing criterion defined, realizing the control on a non-linear system presents its challenges. To overcome these challenges, the researchers have used a Linear Inverted Pendulum Model (LIPM) to linearize the system and simplify the dynamics equations. (Kajita et al. 2001)

Pushing a trolley is one of the tasks that can humanoid robots realize which can be seen in everyday life and industrial circumstances. With an upper body manipulation task, external forces are exerted on the robot’s arms, disturbing its balance and creating. Real time gait generation with feedback from the hand reaction force is realized by on-line modification of gait pattern generation. The proposed method allows for stably pushing an object with varying masses using HRP-2. (Harada et al. 2001) Another method for real-time gait planning for pushing motion was to modify ZMP and cycle time by evaluating the reaction force at the end effector. (Motoi, Ikebe & Ohnishi, 2007) An enhanced LIPM which includes the dynamics model of the cart-load system was proposed to enable for pushing a heavy mass on a trolley. (Hawley & Seulaiman 2017)

This thesis proposes a reference generation and control techniques that are applied for the legs and arms of the humanoid robot. Walking reference trajectories are based on Zero Moment Point Criterion. The main goal of the proposed method is to allow the robot to push a trolley forward couple of times in back-to-back manners while walking in between the pushing motions. When hands are in contact with the trolley, a foot-ground interaction force controller enhances body posture control. Hands are subject to position control when not contacting and are controlled via hybrid position-force control during the pushing motion of the trolley.

The motion begins by a position-controlled walk towards the trolley with hands positioned in front of the body of the robot. When hands make contact with the trolley walking stops and position-force hybrid controlled pushing motion begins. The pushing of the trolley continues until a pre-determined displacement of trolley is reached. After pushing motion is completed hands are retreated back to its home position, and walking starts. Due to the cyclic nature of the motion these steps are repeated.

The next chapter presents a survey on developed humanoid robots and full-body motion control techniques. Chapter 3 describes the simulation environment framework. A reactive force control scheme is proposed in Chapter 4. A ZMP based walking reference generation is described in Chapter 5. Chapter 6 presents the arm hybrid position-force controller for pushing motion. Chapter 7 describes the controller coordination for the algorithm. Chapter 8 includes screenshots and plots from the animation and discusses the results of this thesis. Chapter 9 gives the conclusion with some possible future works.

2. SURVEY OF HUMANOID ROBOTS

2.1. History of Biped Robots

Starting from 1960’s researches have began to grow interest in humanoid robots. Prior to developments of humnaoid robots first man to draw a sketch of an humnaoid robot was Leonardo Da Vinci in 1495. The design of this object was intended for it to be able to sit upright, move its arms and head, and open and close its jaw. (Akhtaruzzaman, 2010)

History of Biped Robots section is going to be divided into 4 parts by their developer. This survey collects the humanoid robots which are developed by Waseda University, Beijing Institute of Technology (BIT), Boston Dynamics, Honda and Humanoid Robotics Project (HRP).

2.1.1. Waseda University

Waseda University was one of the first institutes that researched humanoid robots starting from 1967. Different series of robots of Waseda University is going to be reviewed.

2.1.1.1. WL

In 1967 Professor Ichiro Kato, a robotics pioneer, conducted research on human mobility and constructed the WL-1 biped walker for lower limbs at Waseda University (Lim & Takanshi 2007). After the first prototype in 1969 WL-3 was developed with an electro-hydraulic servo actuator. It used master-slave control method to walk like a human with a swing and stance phases. WL-5 robot was developed in 1972 with 11 DoF with a bendable body. Pictures of WL-1, WL-2 and WL-3 is given in Figure 2. 1

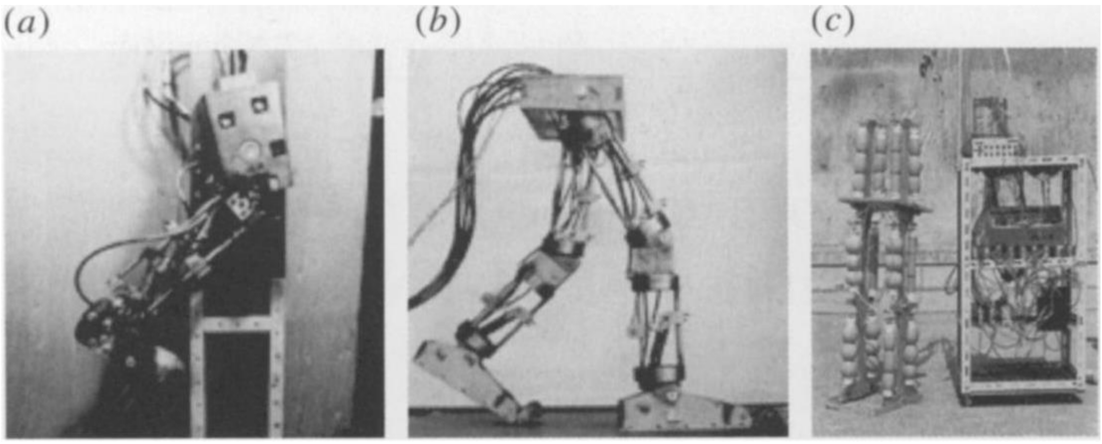

Figure 2. 1 Images of (a)WL-1, (b)WL-2 and (c)WL-3.(Lim & Takanshi 2007)

In 1980, WL-9R was developed with 10 DoF. With a 16-bit microcontroller the robot was able to achieve quasi-dynamic walking for the first time. WL-10R was constructed using a rotary-type servo-actuator to realize forward and backward walking with a speed of 4.4 sec/step in 1983. WL-10DR was developed in 1984 which added torque sensor to the ankle and hip joints. The added sensors allowed WL-10DR to have flexible control during transitioning from one leg to another which resulted in a much faster walking in 1.3 sec/step and 40cm step size. Also, WL-10DR robot was the first every humanoid robot that realized dynamic walking. (Figure 2. 2b) (Takanishi et al. 2010) (Waseda University WL Robots, 2000)

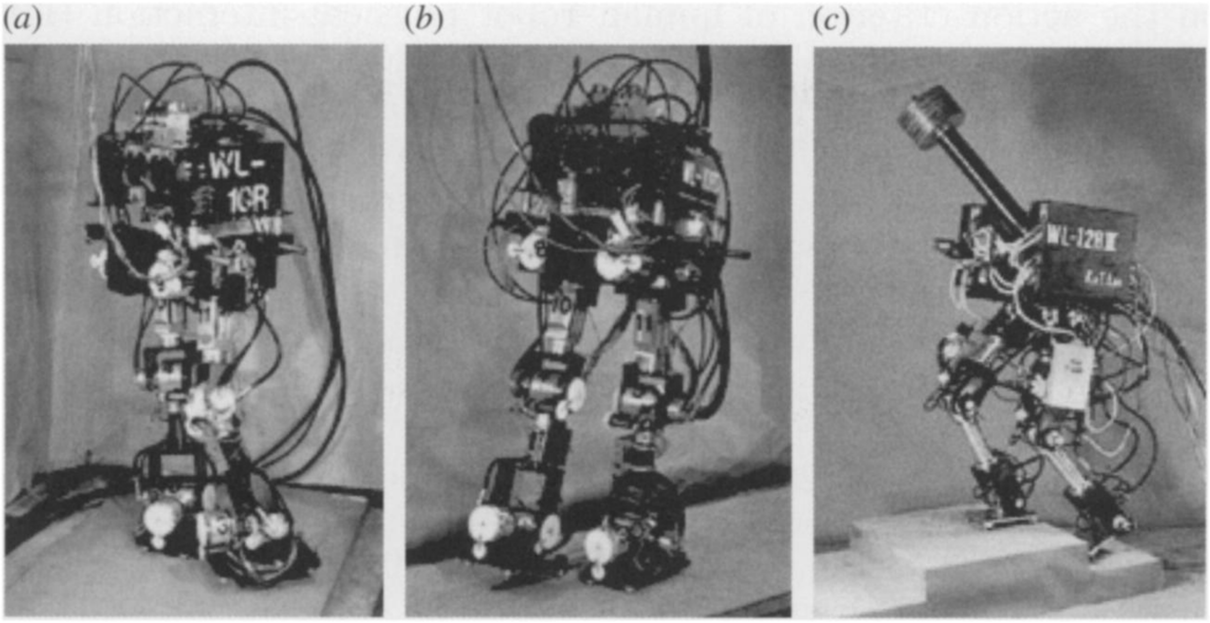

Figure 2. 2 Photos of Biped Robots: (a)WL-10, (b)WL-10DR, WL-12. Lim & Takanshi, 2007)

WL-12, with 2 DoF waist and a trunk was used to simulate motion which resembles more like humans. (Figure 2. 2c) Later in 1990 WL-12 was refined to WL-12III. With a 0.1 m step height and a 10 degrees incline on trapezoidal terrain, it was possible to achieve dynamic walking with a walking period of 2.6 s in steps and 1.6 s on trapezoidal terrain. (Takanishi et al 1990) WL-12RVI and WL-RVII were developed in 1992 and 1995 respectively. They both aimed to improve dynamic walking on unknown terrains.

WL-15 and WL-16 were developed in 2002 and 2004 respectively with a parallel mechanism instead of traditional series mechanism. There are six 1 DoF active linear actuators in the parallel mechanism. First WL-15 displayed the validity of such parallel mechanism by realizing a dynamic biped walking with 200mm step size and a speed of 0.96sec/step. (Sugahara et al. 2002). WL-16 was based on WL-15's design and was able to walk with a step length of 0.3m while carrying a 50kg payload. It is the first ever human carrying humanoid robot. (Sugahara et al. 2004)

2.1.1.2. WAP

In 1969, 1970 and 1971 Waseda University released 3 different humanoid robots named WAP-1, WAP-2 and WAP-3. (Figure 2. 3) respectively. WAP-1 rubber artificial muscles for actuation. Teaching-playback control method was used for planar biped locomotion. WAP-2 had a powerful pouch-type artificial muscle. Pressure sensors on the feet enabled for an automatic posture control. WAP-3 is the first humanoid robot that has the ability to walk on two feet in three dimensions by shifting its center of gravity to the frontal plane.. (Lim & Takanishi 2007)

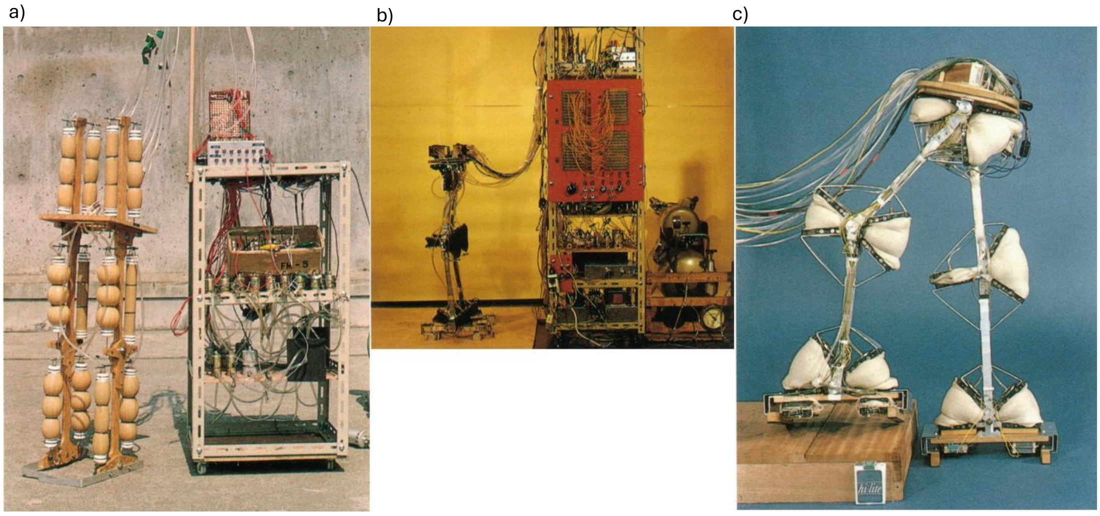

Figure 2. 3 Images of WAP-1(a), WAP-2(b), WAP-3(c)(Takanishi, 2018)

2.1.1.3. WABIAN

In 1996, a robot of adult proportions named WABIAN was created. It used electric motors for actuation and aimed have the same step speed as a human. It can dance with a human and carry goods. It has 35 degrees of freedom. WABIAN-R, WABIAN-RII, WABIAN-RIII and WABIAN-RIV were developed as an improvement of WABIAN in 1997, 1999, 2002 and 2004. (Lim & Takanishi, 2007)

WABIAN-2 was developed in 2005 after WABIAN-RIV. It was developed as a human motion simulator. It features a 2-DoF waist, a 2-DoF trunk, 7-DoF arms, and 7-DoF legs. Waseda University continued to refine WABIAN-2 robot for their experiments. (Waseda University WABIAN-2R, 2013) The images of WABIAN robots are provided in Figure 2. 4

a) b)

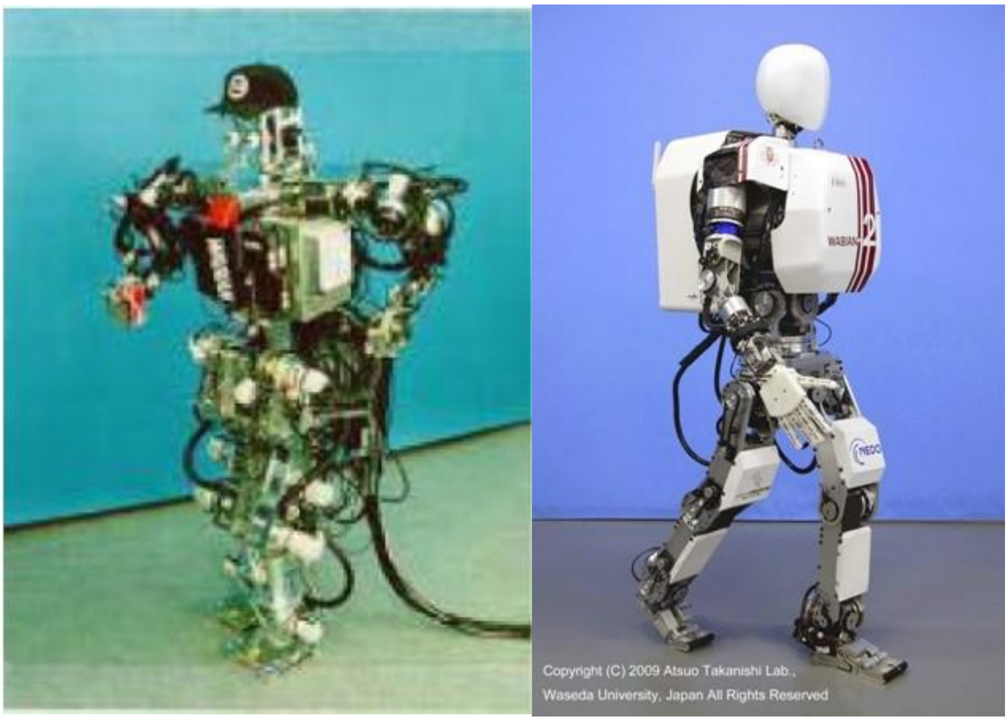

*Figure 2. 4 Images of (a)WABIAN) (b)WABIAN-2***(***Ogura et al. 2006***)**

2.1.1.4. WABOT

The first full-scale anthromorphic robot was WABOT-1, which debuted in 1973. (Figure 2. 5a) In addition to communicating with people in Japanese, WABOT-1 could use external sensors, such as artificial ears and eyes, to gauge an object's distance and direction. It moved more like a shuffle than a walk, but its large feet kept it stable. It was propelled by hydraulics. Additionaly, WABOT-1 was able to realize static walking. (Lim & Takanshi, 2017).

The development of WABOT-2 (Figure 2. 5b) in 1973 aimed to enhance the robot's cognitive abilities, dexterity, and speed of operation. The decision was made to use the keyboard to demonstrate the robot's abilities.. Playing music like an human is an example of activities that require the above mentioned features. A dexterous finger-arm robot with 14 DoF was developed. (Sugano & Kato, 1987)

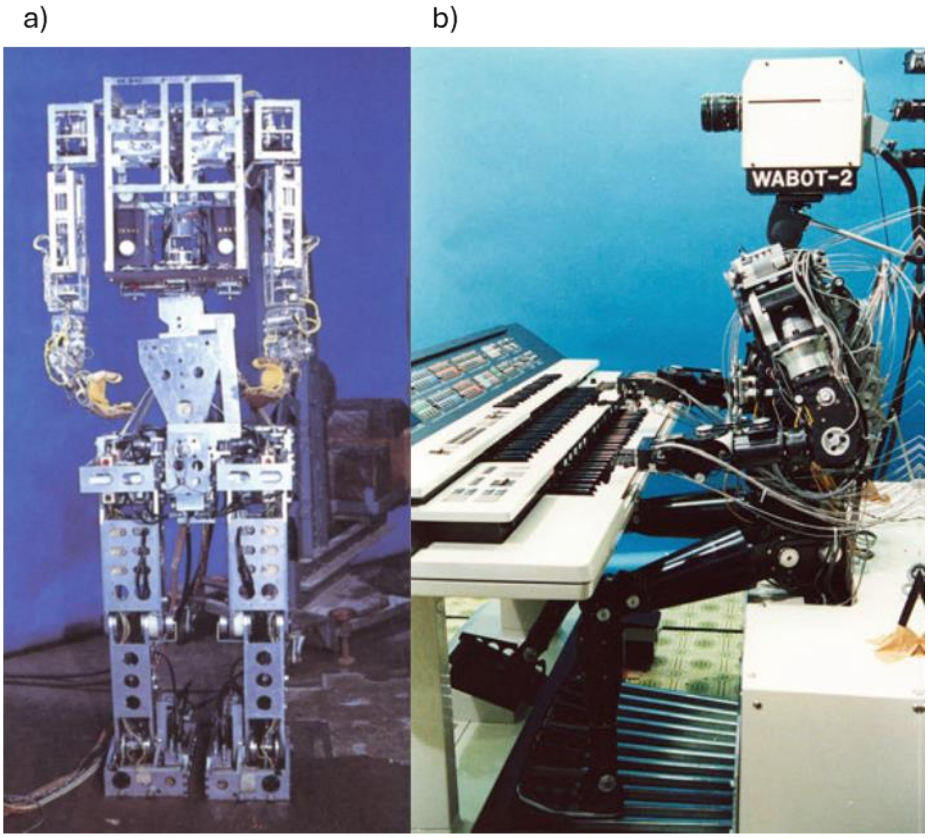

Figure 2. 5 Images of WABOT(a) and WABOT-2(b) (Takanishi, 2018)

2.1.2. HONDA

Honda is mostly known for their automotive industry presence. However, one of the top research firms for humanoid robotics is actually Honda. From 1986 to 2003 different robots were developed for their research towards robots working for human beings. (Figure 2. 6)

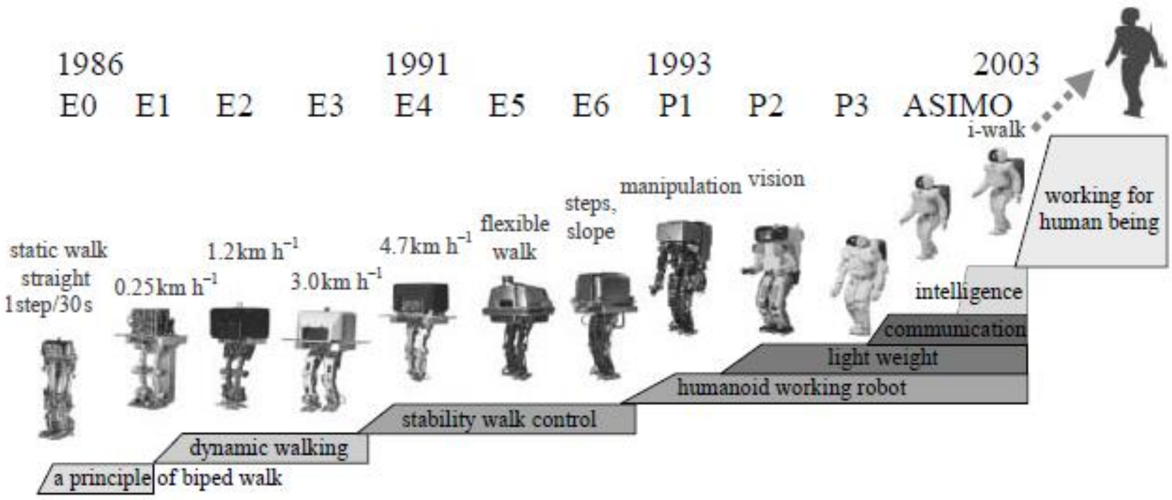

Figure 2. 6 Evolution of a Honda humanoid robot. (Hirose & Ogawa, 2007).

2.1.2.1. E Series

Honda started their humanoid robotics studies in 1986 by developing E0. Main goal was to develop a robot that can walk. As a result, E0 was able achieve static walking with 30sec/step speed. It was very slow but a beginning, nonetheless. With E1 basic joint structure was introduced. The walking speed was increased to 0.25 km/h. Honda's first dynamic walking robot was called E2. Walking on a level surface, its pace was 1.2 km/h. E3 achieved a walking pace of three kilometers per hour. (Hirose & Ogawa, 2007)

Between 1991-1993 Honda developed E4, E5 and E6. Throughout these robots stabilized walking was realized. E6, the last robot of E series, was able to achieve autonomous control of balancing when climbing up and down through stairs, slopes and obstacles. (HONDA Robotics, 2008)

2.1.2.2. P Series

Between 1993-1997 Honda developed man-like humanoid robots. P1 was a robot that could perform upper body tasks like picking up and carrying objects, grabbing doorknobs, and turning on and off electrical and computer switches. (HONDA Robotics, 2008).

The first two-legged, self-regulating humanoid robot in history was called P2. It was possible to push trolleys, walk on uneven terrain, avoid collisions, and adjust for external forces with a 34 DoF setup. However, P2 was too large and heavy, resulting only 15-minute operational time due to high energy consumption of motors. (Hirose & Ogawa, 2007)

With P2’s shortcomings, P3 was developed to address them. The size and weight were reduced. P2 was 1820mm and 210kg, With P3 the size and weight has been reduced to 1600mm and 130kg. Hence the robot was able to operate for longer and better suit human environments. (HONDA Robotics, 2008)

2.1.2.3. ASIMO

Honda’s vision with their humanoid robot R&D was to create a new form of mobility that could be of practical help to humans. (Hirose & Ogawa, 2007). With 28 DoF and a weight of 52kg more compact and lightweight robot was developed. (Figure 2. 7) (HONDA Robotics ASIMO, 2008) A radio communication network controller was used in conjunction with a frame grabber, PCs for voice recognition and synthesis, image processing, control, and planning to create ASIMO's intelligence system. Two color cameras and two microphones were also added to the system for vision and auditory systems. (Sakagami et al. 2002)

ASIMO is equipped with more advanced walking technology named I-WALK. which can run with 3 km/h speed with a 0.05 seconds of airborne time and walk with a speed of 2.5km/h. (HONDA Robotics, 2008)

A demonstration displayed the capabilities of ASIMO by acting like a receptionist. It was able to detect and approach by finding a track to the visitor, find a track to get to visitor and verbally greet with a gesture, recognize the visitor by face recognition and guide the user to a meeting place after checking his/her details. (Sakagami, 2002) This demonstration displays the Honda's vision for humanoid robots which is creating a robot which can work with humans in our environments.

Figure 2. 7 Image of ASIMO (Forbes ASIMO, 2022)

2.1.3. Humanoid Robotics Project (HRP)

HRP is a project that has been studied on by a couple of different institutes such as HONDA, AIST (National Institute of Advanced Industrial Science and Technology) and Kawada Industries. The main goal of HRP robots were to develop a humanoid robot that can work like a human worker.

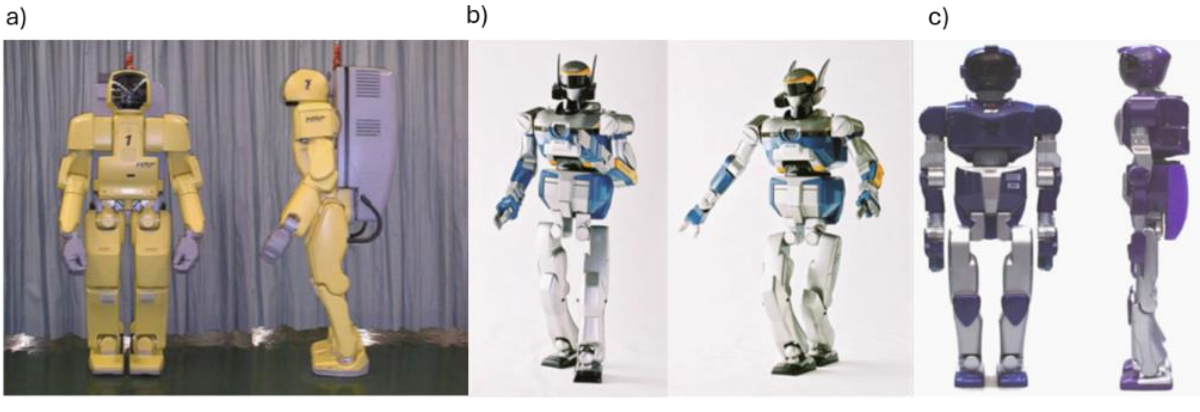

Figure 2. 8 Images of a)HRP-1, b)HRP-2 and c)HRP-2P(Kajita, 2019)

2.1.3.1. HRP-1

The humanoid robot HRP-1 weighs 116 kg, with a height of 1600 mm, and 30 degrees of freedom. (Figure 2. 8a) The robot is a refined Honda P3 model because it was HONDA R&D who developed this robot. Four versions of HRP-1 were evaluated in various settings, including human care, teleoperations of construction equipment, industrial plant maintenance, and home and workplace security services.. (Kajita, 2019)

2.1.3.2. HRP-2/2P

HRP-2P was developed to realize a task in which the robot should work cooperatively in the open air. The goal was for the robot to construct a prefabricated cottage on the construction site by carrying the wallboard alongside a human worker. (Figure 2. 8c)

2.1.3.3. HRP-2Kai

In order to compete in the DARPA Robotics Challenge Finals, HRP-2Kai was constructed. You can read more about DARPA in section 2.1.5.2. A number of adjustments were made based on the HRP-2 hardware to accommodate the duties involved in the 2013 DRC Trials. On the second day of the DRC Finals, HRP-2Kai completed five tasks out of eight, as seen in Figure 2.9. Team AIST-NEDO placed tenth out of the twenty-three teams that attended. (Kajita, 2019)

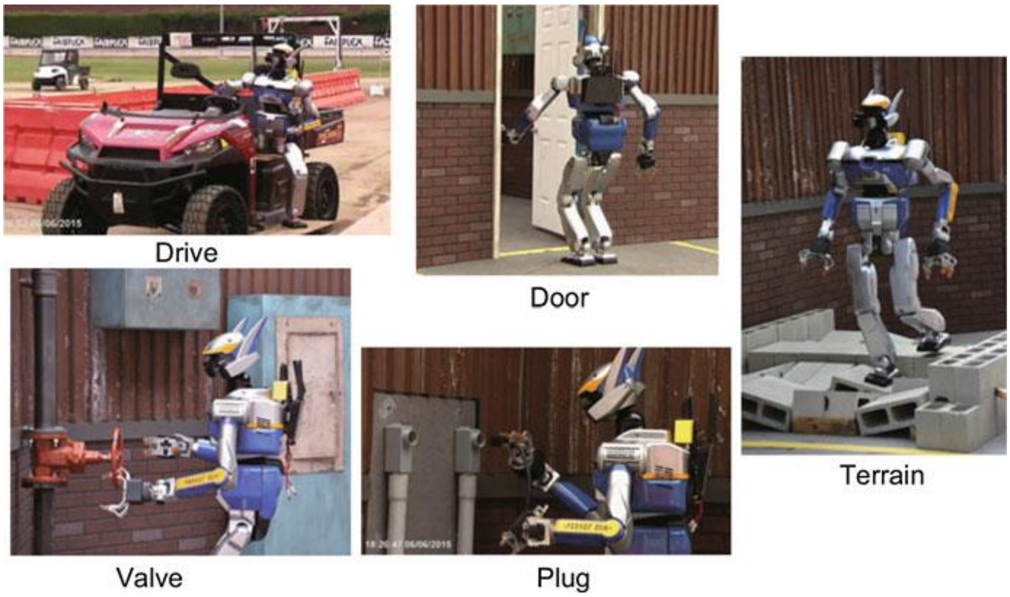

Figure 2. 9 Completed tasks by HRP-2Kai at DRC Finals (Kajita, 2019)

2.1.3.4. HRP-3

The creation of an outdoor humanoid robot as the replacement for the HRP-2 model was the aim of the HRP-3 project. (Figure 2. 10b). In order to function well in outdoor settings, HRP-3 was made to be splash and dust proof. Since the robot's hands and arms were made to manipulate objects more effectively, a redundant system configuration with seven degrees of freedom was selected. (Kajita, 2019)

2.1.3.5. HRP-4C/4

As a synthetic person, HRP-4C was created to better suit entertainment applications like exhibitions. As seen in Figure 2. 10c the robot was 43 kg in weight, 1580 mm tall, and configured in 42 degrees of freedom. Its physical dimensions were created to resemble those of a typical Japanese young woman. The eight servomotors within the head allowed the silicone rubber skin of the face to morph into different expressions. (Kajita, 2019)

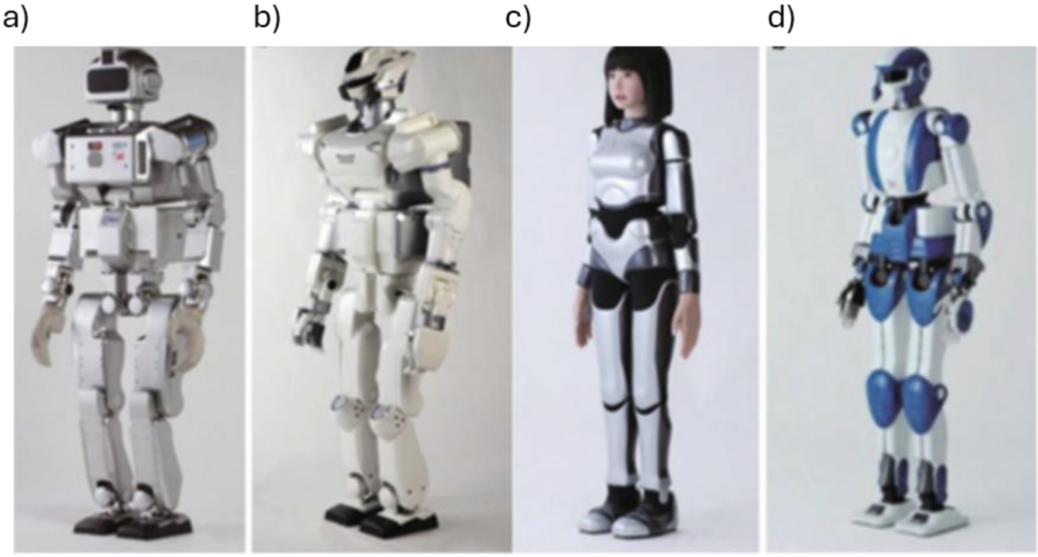

Figure 2. 10 I mages of a)HRP-3P, b)HRP-3, c)HRP-4C and d) HRP-4 (Kajita, 2019)

2.1.3.6. HRP-5P

The most recent iteration of the HRP series, HRP-5P, was created in 2018. intending to make it possible for large-scale assembly businesses like shipyards, airports, and building sites to replace human workers with useful humanoid robots. A gypsum board measuring 910 mm by 1820 mm by 9.5 mm and weighing approximately 11 kg can be skillfully handled with "High Power and Wide Range Joints" and "Suitable Joint Configuration." This served as the primary design objectives. The trial employing HRP-5P also proved that heavy labor with operational humanoid robots on real locations is feasible. (Kaneko et al. 2019) (Figure 2. 11)

Figure 2. 11 Images of HRP-5P performing simple but heavy-duty constructions tasks (ARCH2O HRP-5P, 2024)

2.1.4. Beijing Institute of Technology

In the year 2000, Beijing Institute of Technology (BIT) initiated the study of humanoid robots and established a research group, with Prof. Qiang Huang serving as the team leader. They developed a series of humanoid robots called BHR. The Beijing Institute of Technology Humanoid Robots is the source of the abbreviation BHR.

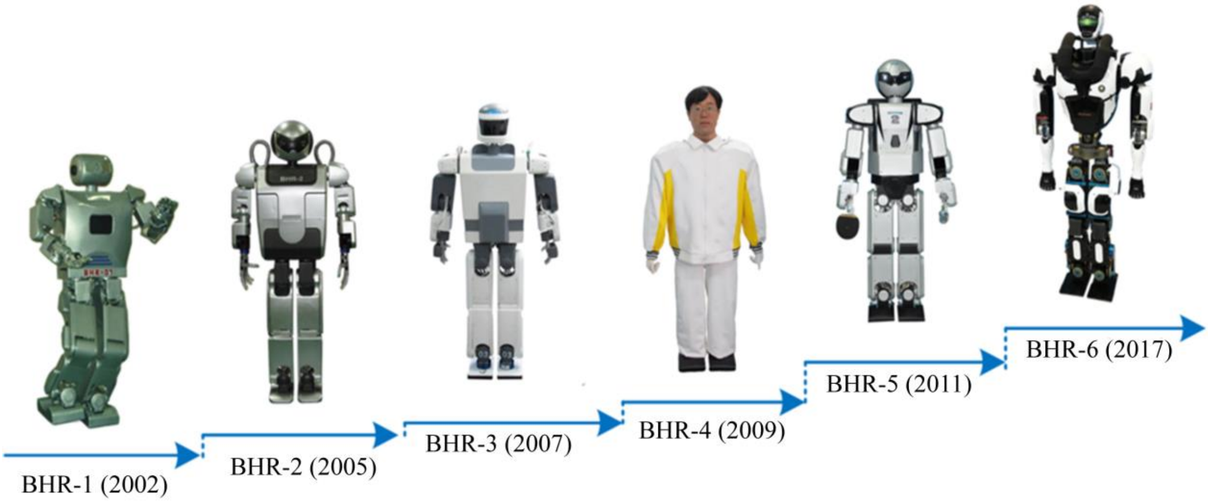

Figure 2. 12 BHR Humanoid Robots From BIT (Huang et al. 2019).

2.1.4.1. BHR-1

The first fully integrated humanoid, known as BHR-1, that can walk dynamically without a leash was created by BIT. It weighed 76 kg and had a height of 1580 mm. It had a 28 degree configuration, gyro, acceleration, force, torque, and vision sensors in its feet and chest. It was used to whole-body control and bipedal walking. It could walk at a pace of 2km/h. (Huang et al. 2019)

2.1.4.2. BHR-2

Complex motion, like that of traditional martial arts like Tai Chi and broadsword, was made possible with BHR-2. The robot weighed 63 kg and measured 1600 mm in length with 32 degrees of freedom. In accordance with the methodology suggested in this research, BIT used BHR-2 to assess the pushing manipulation that occurred during dynamic walking. (Huang et al. 2019)

2.1.4.3. BHR-3

2007 saw the unveiling of BHR-3, which was designed with museums in mind. Both the Zhejiang Science and Technology Museum and the Guangdong Science and Technology Center utilized it. It was doing two shows a day. (Huang et al. 2019)

2.1.4.4. BHR-4

BHR-4, developed in 2009, aimed the address the issue of robot-human interaction. To develop a humanoid robot capable of realizing facial expressions 13 DoF were added to the face with a total of 51 DoF. The expressions on the robot's face allows for easy-to-understand intensions and enables better human- robot interaction. (Ma et al. 2016)

2.1.4.5. BHR-5

In 2011, a humanoid robot that is capable of playing table tennis with fast visual systems named HBR-5 was developed. A robot with high rigidity and power output, low weight and inertia, and more sophisticated real-time information sensing and processing capabilities was needed to complete this mission. (Yu et al. 2015)

2.1.4.6. BHR-6

After BHR-5 BIT aimed to develop a robot with multi-mode motion capabilities. In 2013, in collaboration with Takanishi Laboratory of Waseda University BIT, conducted research to realize such a robot. Hence BHR-6 was unveiled. Multi-mode motion feature of the robot was addressed to solve the issue that arise when robots require to replace humans in dangerous environments such as emergency rescue scenarios. To able to navigate through unknown challenges and not fall a multi-mode motion was proposed. The multi-mode motion includes actions such as crawling or jumping. (Huang et al. 2019)

2.1.5. Boston Dynamics

Boston Dynamics is one of the leading research companies that exist currently. Their robots are commercially used in various sectors. Their humanoid research has started with PETMAN and continues with ATLAS.

2.1.5.1. PETMAN

A humanoid robot named PETMAN was created to test protective gear against chemicals. (Figure 2. 13c) Chemical sensors were implemented on the robot to measure the exposure to chemical agents under the Individual Protective Equipment (IPE). Due to the lack of time for development a different but similar humanoid robot was developed named PetProto. PetProto was developed for studies on control software that would allow a bipedal robot to dynamically balance with a natural, human like gait. (Nelson et al. 2012)

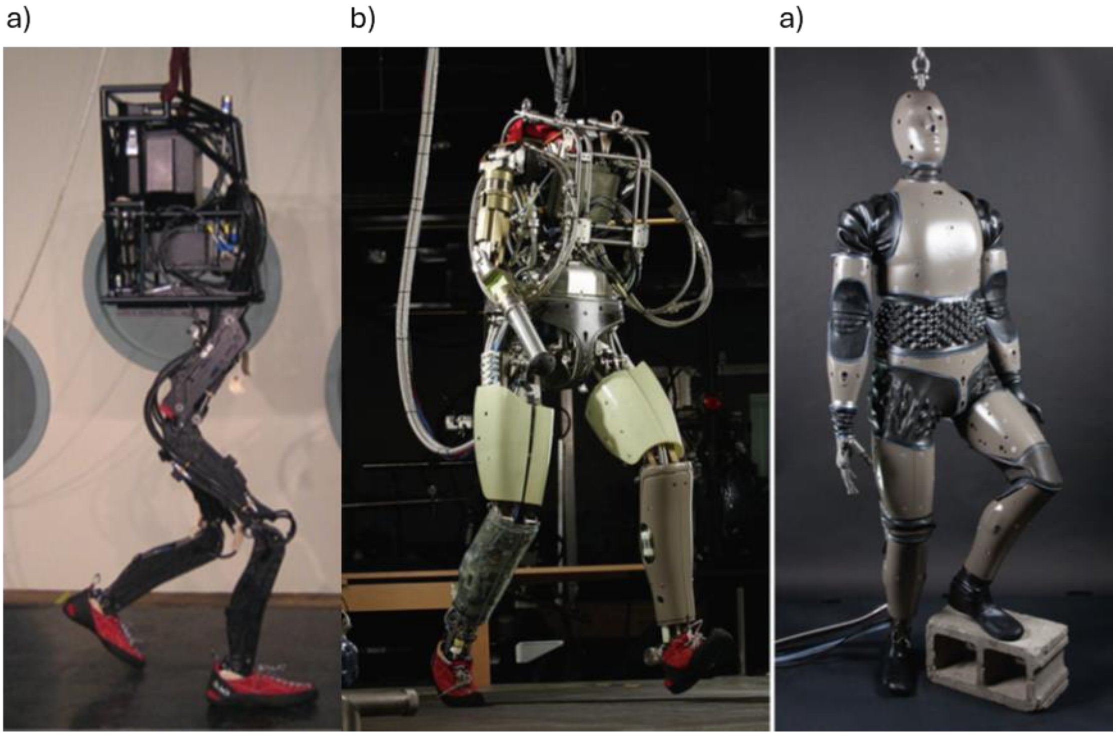

Figure 2. 13Images of PETProto(a), Preliminary version of PETMAN(b), Final version of PETMAN(c) (Nelson, Saunders & Playter, 2019)

PETProto took 4 months to build, and dynamic heel-to-heel bipedal walking was realized. It was able to walk with 7.2 km/h speed. (Figure 2. 13a) Both PETProto and PETMAN uses the same walking control architecture which allowed for 4.8km/h walking speed for PETMAN.

PETMAN has a configuration with 29 DoF. Number of degrees of freedom were decided during the design phase of the project by using motion capture data collection with human motions such as jumping jacks, walking, sitting, transitioning from standing to prone, crawling and other typical soldier tasks. (Nelson, Saunders & Playter, 2019)

2.1.5.2. ATLAS

ATLASProto was introduced in 2012. The PETProto concept only needed arms added by the mechanical design. PETProto now has six DoF in total. The forearm's springs and sensors made it possible to sense while in contact with the surroundings. By swinging or supporting the body by making touch with its surroundings, the added arms helped the robot maintain its overall balance. (Nelson, Saunders & Playter, 2019)

Atlas was created by combining the legs of PETMAN with a less complex upper body, flexible shoulders, and arms resembling clubs. One of the most significant hardware changes was to implementing CoP sensing feet implementation. This change allowed for much better stability. (Figure 2. 14) With the new developments ATLAS was able to achieve balance on wide array of terrain. (Nelson, Saunders & Playter, 2019)

Figure 2. 14 Images of ATLAS walking on unknown environments (Nelson, Saunders & Playter, 2019)

Defense Advanced Research Facility Projects Agency (DARPA) held trials for humanoid robots where they executed various different tasks. The development for this competition started in 2012. DARPA funded Boston Dynamics to build copies of ATLAS-DRC which was a redesign of PETMAN. (Figure 2. 15) These copies would be supplied to teams selected to compete in the DRC. Boston Dynamics provided an Application Programming Interface (API) to the teams that were using ATLAS-DRC for the competition.

In 2015 DARPA finals were held. The humanoid robots that were competing were required to complete a set of tasks within 1 hour. An emergency scenario was created for these robots. The scenario consisted of an emergency scenario which the robots have to drive a vehicle to a destination, get out of the vehicle, open a door to the building where communications breakdown, turn a valve, cut a hole in the wall and get over a pile of debris and climb a set of stairs. To be able to support DARPA finals Boston Dynamics developed ATLAS-Unplugged. (Nelson, Saunders & Playter, 2019)

Boston Dynamics' first untethered robot was named ATLAS-Unplugged. (Figure 2. 15b) Atlas had to redesign over 75% of it. The arms were given a 7th DoF to increase the useful space. The actuation type of the neck and three forearm degrees of freedom was switched from hydraulic to electric. (Feng et al. 2015)

Figure 2. 15 Images of (a)ATLAS-DRC and (b)ATLAS-Unplugged (Nelson, Saunders & Playter, 2019)

Boston Dynamics provided ATLAS-DRC or ATLAS-Unplugged support to seven distinct DRC teams. As per the support arrangement, Boston Dynamics was not able to participate in the DRC. Nevertheless, ATLAS-Unplugged was utilized by three of the top seven teams, demonstrating the robot's capabilities.

From 2016-2024 Boston Dynamics has released multiple videos regarding the Atlas performing various tasks. These tasks include different scenarios such as picking up moving boxes, walking on snowy terrain, opening doors, jumping, backflipping, running on uneven terrain, doing a gymnastics routine, completing a parkour with varying obstacles and even helping humans in a construction site by moving different tools.

Every Atlas prototype up until 2024 was a hydraulic robot. Boston Dynamics unveiled their all-electric take on the humanoid robot. According to the manufacturer, the new model's improved swiveling joints enable it to perform jobs that are hazardous, unclean, or tedious like no other. More range of motion and greater strength than any of the previous generations will be features of the new model. New AI and machine learning tools has been implemented like reinforcement learning and computer vision to operate in complex real-world situations. (Boston Dynamics 2024)

2.2. Survey on Full- Body Motion Control

Balance in biped robotics is one of the most important features in its control. Achieving balance on its own is a challenging issue, when additional disturbances are introduced with manipulation by the upper body, it gets even more complicated. Biped robot locomotion includes 2 different phases according to the ground contact, single support and double phase. While the double support phase has both of its feet in contact with the ground and is an over-actuated system, the single support phase only has one foot in contact with the ground. (Chevallereau et al. 2009). The goal of humanoid robotics is to create machines that can operate just like humans with human-like intelligence. (Sugihara & Morisawa, 2020). To realize such a task naturalness is an important aspect which has been researched before (Erbatur & Kurt, 2002).

First balancing criterion is CoM (Centre of Mass) and CoP(Centre of Pressure) is the first balancing criterion. From an intuitive and scientific perspective, any 3D object is in a stable state if its center of mass is inside the support region. (Cholewiak, Fleming & Singh, 2015). In the context of biped robots, if the CoM trajectory is adjusted well stable walking of the robot can be realized even with presence of disturbances. (Jing & Zheng, 2020). There are methods such as preview control where the CoM is predicted, and a smoother motion is achieved. (Shimmiyo et al. 2013) Dynamic Balance Force Control was realized by using COM motion planner for compliant humanoid robots. (Stephens & Atkenson, 2010).

Second balancing criterion is the Zero-Moment-Point. ZMP is one of the most widely used stability criterion. Harada defined ZMP as a point on the ground at which the tangential component of the moment generated by the ground reaction force/moment becomes zero. (Harada et al. 2003) Just like in COM stability criterion if the defined point lies within the convex hull of the foot supporting area, the robot is in stability.

Also Generalized Zero Moment Point was defined just like ZMP however, the reaction force from the hands is not included in the calculation. Hence ZMP and GZMP are equal to each other in case of no hand contact with the environment. GZMP is used for the stability criterion in case of upper body manipulation. (Harada et al. 2006)

Galdeano suggested a third order spine function to generate hip and foot trajectories for stable dynamic walking, based on the ZMP stability criterion. (Qiang et al. 1999)

Inverted pendulum model method (IPM) was used a dynamic model where ZMP constraints are analyzed in the IPM motion. COG is also approximated by the IPM. (Tang & Er, 2007) This method simplifies the dynamic model by considering single mass and massless legs. IPM was further extended by Albert and Gerth when they proposed Two-Mass Inverted Pendulum and Multiple Mass Inverted Pendulum. (Albert, Gerth, 2003)

Linear Inverted Pendulum is one of the most common models that is used in humanoid robotics research field since it gives a simple mathematical illustration of a walking robot on two legs. It is an expansion of the IPM in which the torso's height is taken into account in a fixed manner. (Kajita et al. 2001). Due to its linear dynamics a simple model can be created. There are multiple researches where LIPM and ZMP are used together for gait generation.

In order to increase dynamic walking stability, a ZMP-based optimization was added to a three-mass linear inverted pendulum model. ZMP based optimization. By using the humanoid robot SHERPA, the effectiveness has been presented. (Galdeano et al. 2016).

By using preview control of ZMP and a LIPM of the robot, gait generation was also proposed. The method first introduces a convenient cart-table representation to design a ZMP controller. Later the ZMP based walking generation method was formalized as a ZMP tracking servo controller. (Kajita et al. 2003). It was demonstrated that preview control could effectively make up for the discrepancy between the accurate multi-body model and the reduced cart-table model using a simulation of the HRP-2P humanoid robot.

For human like motion, ZMP trajectory from human walking data based on the concept of Divergent Component of Motion (DCM) can be mimicked. A combination of, LIPM and a trajectory generation based on using DCM and COM natural fast biped walking can be achieved. In this case, WALKER+ humanoid robot was used for experimental results. (Wang et al. 2018).

The control technique called Model Predictive Control can handle strict limitations on states and controls. (Mayne et al. 2000). And by nature, biped robots rely on their contact forces on their which are severely limited. A static walking biped robot which uses Model Predictive Control. (Azevedo, Poignet & Espiau, 2002). MPC was also used by Wieber with a HRP-2 humanoid robot simulation to deal with strong perturbations by minimizing the jerk of the trajectory of the CoM which is approximated by the LIPM. (Wieber, 2006)

A third balance criteria was proposed by AIST. This method checks if the sum of the gravity and the inertia wrench applied to the COG of the robots is inside the polyhedral convex cone of the contact wrench between the feet of a robot and its environment. It also improves the stability of the robots while gaiting on stairs or rough terrain. It was demonstrated that when the robot moves on a horizontal floor with enough friction, this approach meets the ZMP balancing condition. (Hirukawa, 2006)

To further improve balance in difficult settings, the aforementioned criterion can also be utilized to account for sliding in the horizontal plane and rotation along the vertical axis (yaw). In a situation where either the sliding or yaw effects are observed ZMP is necessary but not sufficient. With Contact Wrench Cone approach ZMP criterion is also satisfied, and further improvements are made. (Navaneeth & Joy, 2022)

Upper body control with gait pattern generation has been an important research topic on humanoid robots. If the task of the desired robot is to manipulate objects and work with humans on uncontrolled environments, upper body control is a requirement. The fact that gaiting in an unknown environment and interacting with an object poses multiple challenges such as large uncertainty of unstructured environments. (Sarıyıldız & Ohnishi, 2013). As this paper discusses pushing an object can be an important task that a humanoid robot can do.

Real time gait generation with feedback from the hand reaction force is realized by on-line modification of gait pattern generation. (Harad et al. 2007). By controlling the arms using impedance control and analytically obtaining COG very fast and calculating new COG trajectory for smooth operation. Gaiting and pushing states are separated, walking distance is equal to the pushing amount where force control is applied.

a real-time gait planning that adjusts the ZMP and cycle time, which are determined by the force applied to the arms, in order to push an unknown item. The impact of response force on the hands modifies the ZMP trajectory. This technique is used for pushing throughout both the single and double support phases. (Motoi, Ikebe & Ohnishi, 2007)

Advanced automatic and Bilateral control methods for both gaiting and pushing an unknown object was reached. With both advanced automatic and bilateral control walking on uneven terrain and pushing on unknown object was realized. Advanced motion control is used to realize human's Daily activities such as walking on uneven terrain. To performs dexterous and versatile tasks like humans, bilateral control was used with a force sensor on the end effector of the robot, its hands. (Sarıyıldız & Temeltaş, 2017)

The SARCOS robot, which has an inbuilt camera, was utilized for research purposes to perform a baseball-batting activity. With consideration for bipedal balancing, the control superposes quick and fluid batting trajectories on a whole-body force controller. In the face of unknown external forces, the robot was able to successfully complete compliant full-body balancing tasks thanks to the implementation of a precise torque controller and a whole-body force controller. Cheng et al. (2006)

3. DYNAMICS EQUATIONS AND FRAMEWORK OF THE SIMULATION

Let x, v, u represent generalized coordinates, velocity, and force, respectively.

$$\mathbf{x}^T = [\mathbf{p}_B^T, \mathbf{A}_B^T, \boldsymbol{\theta}^T] \in R^3 \times SO(3) \times R^N \tag{3.1}$$

$$\mathbf{v}^T = [\mathbf{v}_B^T, \mathbf{w}_B^T, \mathbf{w}^T] \in R^3 \times R^3 \times R^N \tag{3.2}$$

$$\mathbf{u}^T = [\mathbf{f}_B^T, \mathbf{n}_B^T, \boldsymbol{\tau}^T] \in R^3 \times R^3 \times R^N \tag{3.3}$$

where

$\boldsymbol{p}_B$: 3×1 vector specifying base-link position

$\boldsymbol{A}_B$: 3×3 matrix specifying base-link attitude

$\boldsymbol{\theta}$: $N\times1$ vector specifying joint angle

$\boldsymbol{v}_B$: 3×1 vector specifying base-link velocity

$\boldsymbol{w}_B$: 3×1 vector specifying angular velocity of base-link

$\boldsymbol{w}$: $N\times1$ vector specifying joint angular velocity

$\boldsymbol{f}_B$: 3×1 force vector generated in base-link

$\boldsymbol{n}_B$: 3×1 torque vector generated in base-link

$\boldsymbol{\tau}$: $N\times1$ torque vector generated by actuator

N : Number of joints of the robot

The relationship between the link axes and the world axes is specified by the transformation matrix $\boldsymbol{A}_B$. The following are the motion equations for the robot

$$\dot{\mathbf{p}}_B = \mathbf{v}_B \tag{3.4}$$

$$\dot{\mathbf{A}}_B = \mathbf{w}_B \times \mathbf{A}_B \tag{3.5}$$

$$\dot{\boldsymbol{\theta}}_B = \mathbf{w} \tag{3.6}$$

and

$$\mathbf{H}(\mathbf{x})\dot{\mathbf{v}} + \mathbf{C}(\mathbf{x}, \mathbf{v})\mathbf{v} + \mathbf{g}(\mathbf{x}) + = \mathbf{u} + \mathbf{u}_E \tag{3.7}$$

where

$\boldsymbol{H}(\boldsymbol{x})$: $(N+6)\times(N+6)$ inertia matrix

$\boldsymbol{C}(\boldsymbol{x},\boldsymbol{v})$: $(N+6)\times(N+6)$ matrix specifying centrifugal and Corioli’s effects

$\boldsymbol{g}(\boldsymbol{x})$: $(N+6)\times1$ vector specifying gravity effect

$\boldsymbol{u}_E$: $(N+6)\times1$ vector specifying generalized forces generated by external forces

A general form of a dynamic equation is given in (3.7). The suggested technique makes use of a simulation environment that leverages the actuator torque inputs to numerically calculate the angles of joints and the body position in each time step. The following definitions provide an explanation of the steps needed in modeling the biped system. Every step time, Euler integration updates the generalized states (x,v).

$$\mathbf{p}_B(t+h) = \mathbf{p}_B(t) + h\mathbf{v}_B(t) \tag{3.8}$$

$$\mathbf{A}_B(t+h) = \mathbf{T}(h\mathbf{w}_B)\mathbf{A}_B(t) \tag{3.9}$$

$$\theta(t+h) = \theta(t) + h\mathbf{w} \tag{3.10}$$

$$\mathbf{v}(t+h) = \mathbf{v}(t) + h\dot{\mathbf{v}}(t) \tag{3.11}$$

$$\dot{\mathbf{v}}(t) = \mathbf{H}(\mathbf{x}(t))^{-1}\left[\mathbf{u}(t) - \mathbf{u}_E(\mathbf{x}(t), \mathbf{v}(t)) - \mathbf{b}(\mathbf{x}(t), \mathbf{v}(t)\right] \tag{3.12}$$

where the biasing vector $\mathbf{b}(\mathbf{x}(t), \mathbf{v}(t))$ is defined as (3.13)

$$\mathbf{b}(\mathbf{x}(t), \mathbf{v}(t)) = \mathbf{C}(\mathbf{x}(t), \mathbf{v}(t))\mathbf{v}(t) + \mathbf{g}(\mathbf{x}(t)) \tag{3.13}$$

(3.8) to (3.13) provides a description of numerical integration for the simulation.

(3.9) describes the rotating transformer $\mathbf{T}(h\mathbf{w}_B)$, whose angle around the $\boldsymbol{w}_B$ axis is $h|\boldsymbol{w}_B|$. In response to the angular velocity of the base link, it modifies the orientation matrix of the base link. It is obtained through:

$$\mathbf{T}(h\mathbf{w}_B) = \left[(\cos\psi)\mathbf{I}_3 + (1-\cos\psi)\mathbf{r}\mathbf{r}^T + (\sin\psi)\left[\mathbf{r}\times\right]\right] \tag{3.14}$$

where, $\psi = h|\mathbf{w}_B|$, $\boldsymbol{I}_3$ is 3×3 identity matrix, and $\boldsymbol{r} = \boldsymbol{w}_B / |\boldsymbol{w}_B|$.

Based on the position, velocity, and acceleration of the joint angles, the simulation computes the joint torque trajectories, and the contact forces from the ground. Therefore, the primary goal of this framework is to generate the joint torque τ and external force U_E utilizing the numerically integrated generalized coordinates x, velocities c, and acceleration $\dot{v}$.

The simulation calculates the contact forces from the ground as well as the joint torque trajectories based on the position, velocity, and acceleration of the joint angles. Thus, the main objective of this framework is to produce the joint torque τ and external force U_E by using the generalized coordinates x, velocities x, and acceleration $\dot{v}$ that are numerically integrated.

The Newton-Euler iterative formula which was proposed in 1980 can be utilized to obtain the inertia matrix, $\boldsymbol{H}(\boldsymbol{x})$, and the biasing vector, $\boldsymbol{b}(\boldsymbol{x},\boldsymbol{v})$. For simplification, both inertia matrix, $\boldsymbol{H}(\boldsymbol{x})$ and biasing vector, $\boldsymbol{b}(\boldsymbol{x},\boldsymbol{v})$, neglects the Corioli's, centrifugal, gravitational and external forces. The inertia matrix, $\boldsymbol{H}(\boldsymbol{x})$, is computed numerically by solving the inverse dynamics with x equal to the current state $\dot{\boldsymbol{v}} = \boldsymbol{e}_j$ for $1 \le j \le N+6$ where $\boldsymbol{e}_j$ denotes a unit vector with all elements set to zero except the j^{th} element, set to one. This setup allows for calculation of j^{th} column in each iteration. The symmetric characteristics of the inertia matrix can be used for more efficient calculation. The biasing vector, $\boldsymbol{b}(\boldsymbol{x},\boldsymbol{v})$, is computed numerically by solving the inverse dynamics with (x,v) set to the current state and $\dot{\boldsymbol{v}} = 0$.

By solving the inverse dynamics with equal to the current state $\dot{\boldsymbol{v}} = \boldsymbol{e}_j$ for $1 \le j \le N+6$ where $\boldsymbol{e}_j$ represents a unit vector with all elements set to zero except the j^{th} element, which is set to one, the inertia matrix, $\boldsymbol{H}(\boldsymbol{x})$, can be obtained numerically.

Let u_a be equal to the generalized forces generated by the inertial, centrifugal, Corioli's and gravity forces which can be calculated by setting the external forces $f_E = 0$ and rewriting (3.7).

$$u_a(x,v,\dot{v}) = H(x)\dot{v} + C(x,y) + g(x) \tag{3.15}$$

The last problem is figuring out how to compute the external force vector, or f_E, in order to describe the forces of environmental interaction. This paper thesis uses an adaptive penalty-based technique which was proposed by Erbatur by reducing the kinetic energy of the bodies contact. The generalized external force, u_E, can be obtained after the external force vector, f_E, has been generated.

Finding a way to calculate the external force vector, or f_E, to represent the forces of environmental contact is the final challenge. Erbatur's adaptive penalty-based approach, which lowers the kinetic energy of the body's touch, is used in this paper thesis. Once the external force vector, f_E, has been created, the generalized external force, u_E, can be found.

$$u_E = \sum_{j \in M_A} K_j F_{E_j} = K f_E \tag{3.16}$$

where

$$M_A = \bigcup_{i=1}^{N} M_i \tag{3.17}$$

K_j: $(N+6)\times 3$ matrix specifying transforms from j^{th} external force to generalized forces

M_A: A set of index numbers of all active contact points

f_E: $(3M)\times 1$ vector which contains active contact forces

K: $N+6\times(3M)$ matrix specifying transforms from f_E generalized forces

M : Number of time-variant active contact points

Now, (3.7) and (3.16) can be rewritten as

$$u_A = u + K f_E \tag{3.18}$$

K can be calculated by solving the inverse dynamics, ignoring the effects of gravity, centrifugal force, and Coriolis, and using x equal to the present state, $f_E = e_j$, and $\dot{v} = 0$. Now, (3.18) is rewritten as:

$$\begin{bmatrix} f_A \\ n_A \\ \tau_A \end{bmatrix} = \begin{bmatrix} f_B \\ n_B \\ \tau \end{bmatrix} + \begin{bmatrix} K_f \\ K_n \\ K_\tau \end{bmatrix} f_E \tag{3.19}$$

where f_B and n_B stand for the force and moment, respectively, applied to the origin of the base link. The previously outlined process establishes the joint torques in the computer simulation program.

The kinematic and dynamic parameter of the robot SURALP designed at Sabancı University are used in the simulations. Figure 3. 1 and Table 3.1 presents description of this humanoid robot.

Upper Leg Length	280mm
Lower Leg Length	270mm
Ankle Center to Foot Sole Distance	124mm
Foot Dimensions	240mm $\times$ 150mm
Upper Arms Length	219mm
Lower Arms Length	255mm
Robot Weight	114kg

Table 3.1. Dimensions and weight data of SURALP

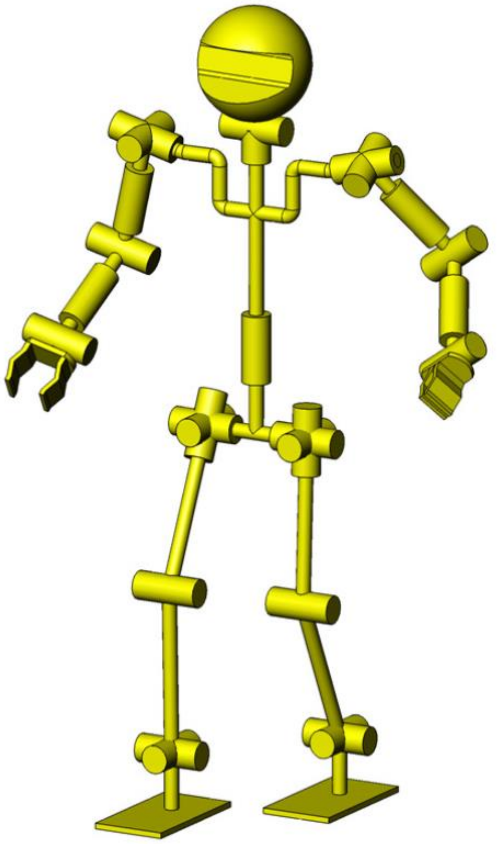

Figure 3. 1 Kinematic arrangement of SURALP

The trolley is represented by a 25 kg mass on the ground with viscous and Coulomb friction effects. The interaction of feet with ground and hands with the trolley are modeled by spring and damper models.

Figure 8. 2 displays a snapshot from the animation window.

4. REACTIVE FORCE CONTROL SCHEME

(3.7) provides the universal biped dynamical equation. By dissecting the definition of biasing vector provided in (3.13) for body and leg dynamics, the following equation may be created.

$$\begin{bmatrix} \mathbf{H}'_{11} & \mathbf{H}'_{12} & \mathbf{H}'_{13} \\ \mathbf{H}'_{21} & \mathbf{H}'_{22} & \mathbf{H}'_{23} \\ \mathbf{H}'_{31} & \mathbf{H}'_{32} & \mathbf{H}'_{33} \end{bmatrix} \begin{pmatrix} \dot{\mathbf{v}}_B \\ \dot{\mathbf{w}}_B \\ \ddot{\theta} \end{pmatrix} + \begin{pmatrix} \mathbf{b}'_1 \\ \mathbf{b}'_2 \\ \mathbf{b}'_3 \end{pmatrix} + \begin{pmatrix} \mathbf{u}_{E_1} \\ \mathbf{u}_{E_2} \\ \mathbf{u}_{E_3} \end{pmatrix} = \begin{pmatrix} \mathbf{0} \\ \mathbf{0} \\ \tau \end{pmatrix} \tag{4.1}$$

where

H'_{ij} : Sub-matrices of the $H'\ (x)$ matrix representing the robot's inertia where $(i, j) \in (1,2,3)$

v_B : The linear velocity of the robot's coordinate frame with respect to a fixed world coordinate frame.

w_B : The angular velocity of the robot's coordinate frame with respect to a fixed world coordinate frame.

θ : The vector of the biped robot's joint displacements.

b'_1, b'_2, b'_3 : Sub-vectors of the bias vector $b'(x,v)$.

u_{E1} : Net force impact of the robot body's response forces.

u_{E2} : Net torque impact of the robot body's response forces

u_{E3} : The effect of reaction forces on joints of the robot.

τ : The generalized joint control vector, typically consisting of joint actuation torques for a robot with revolute joints.

$\mathbf{H}'_{11}, \mathbf{H}'_{12}, \mathbf{H}'_{21}$, and $\mathbf{H}'_{22}$ are 3×3 matrices. $\mathbf{H}'_{13}$ is $3\times N$, $\mathbf{H}'_{23}$ is $3\times N$, $\mathbf{H}'_{31}$ is $N\times 3$, $\mathbf{H}'_{32}$ is $N\times 3$, and $\mathbf{H}'_{33}$ is $N\times N$. The need of managing the reactive force to regulate body dynamics is seen in (4.1). Body dynamics are dictated by the response force because it is not directly actuated. One can rewrite the body dynamics from (4.1) as

$$\begin{bmatrix} \mathbf{H}'_{11} & \mathbf{H}'_{12} \\ \mathbf{H}'_{21} & \mathbf{H}'_{22} \end{bmatrix} \begin{pmatrix} \dot{\mathbf{v}}_B \\ \dot{\mathbf{w}}_B \end{pmatrix} + \begin{pmatrix} \mathbf{b}'_1 \\ \mathbf{b}'_2 \end{pmatrix} + \begin{bmatrix} \mathbf{H}'_{13} \\ \mathbf{H}'_{23} \end{bmatrix} \ddot{\theta} + \begin{pmatrix} \mathbf{u}_{E_1} \\ \mathbf{u}_{E_2} \end{pmatrix} = \begin{pmatrix} \mathbf{0} \\ \mathbf{0} \end{pmatrix}. \tag{4.2}$$

$$\begin{pmatrix} \mathbf{u}_{E_{1ref}} \\ \mathbf{u}_{E_{2ref}} \end{pmatrix} = \mathbf{K}'\mathbf{f}_{E_{ref}} \tag{4.3}$$

Where K' is the $6\times(3M)$ sub-matrix of $\boldsymbol{K} = \begin{bmatrix} \boldsymbol{K}' \\ \boldsymbol{K}'' \end{bmatrix}$ which is the transformation matrix that relates the ground interaction forces on the foot to reactive force and torque applied to the robot's body.

To compute for force reference for the foot (4.3) is used, which is an under-determined set of equations. Furthermore, not every system solution is physically feasible because of the non-attractive nature of the contact and the nonslip criterion that must be met for stability. The following are the limitations of the non-slip condition and the non-attractive character of the touch. Let $\boldsymbol{f}_{E_i} = \lfloor \boldsymbol{f}_{E_{ix}} \quad \boldsymbol{f}_{E_{iy}} \quad \boldsymbol{f}_{E_{iz}} \rfloor, \quad i \in \{1,2,\ldots,8\}$.

- Non-attractive nature of contact:

$$\mathbf{f}_{E_{iz}} \geq 0, \quad \forall\, i \in \{1,2,\ldots,8\} \tag{4.4}$$

- Non-slip condition:

$$-\mu \leq \frac{\sqrt{\mathbf{f}_{E_{ix}}{}^2 + \mathbf{f}_{E_{iy}}{}^2}}{\mathbf{f}_{E_{iz}}} \leq \mu, \quad \forall\, i \in \{1,2,\ldots,8\} \tag{4.5}$$

As a nonlinear restriction, the inequality in (4.5) is present. For biped locomotion, an optimization with constraints is employed to compute the set of ground forces. To simplify the optimization process, the non-linear constraint is approximated.

$$\begin{aligned} -\frac{\sqrt{2}}{2}\mu \leq \frac{\mathbf{f}_{E_{ix}}}{\mathbf{f}_{E_{iz}}} \leq \frac{\sqrt{2}}{2}\mu \\ -\frac{\sqrt{2}}{2}\mu \leq \frac{\mathbf{f}_{E_{iy}}}{\mathbf{f}_{E_{iz}}} \leq \frac{\sqrt{2}}{2}\mu, \quad \forall\, i \in \{1,2,\ldots,8\} \end{aligned} \tag{4.6}$$

Despite being a stricter constraint than (4.5), (4.6) is nonetheless in use because of its linear qualities, which make the problem easier to understand. One can rewrite (4.4) and (4.6) in a more condensed manner.

$$A\mathbf{f}_{Eref} \leq 0 \tag{4.7}$$

Where A is a 24×24 matrix derived from the previously stated constraints. Now one can summarize the problem as solving for f_E which minimizes

$$\begin{aligned} &\frac{1}{2}\left\| \mathbf{K}'\mathbf{f}_{Eref} - \begin{pmatrix} \mathbf{u}_{E_{1ref}} \\ \mathbf{u}_{E_{2ref}} \end{pmatrix} \right\|^2 \\ s.t. \quad &A\mathbf{f}_{Eref} \leq 0 \end{aligned} \tag{4.8}$$

The sequential quadratic programming technique is used to solve this linear constrained least-squares problem. This thesis does not provide the optimization specifics, however Rardin, 2017 provides the technique. The optimization algorithm's solution is transformed straight into joint torques by:

$$\mathbf{u}_{E_{3ref}} = \mathbf{K}''\mathbf{f}_{Eref} \tag{4.9}$$

(4.9) has infinitely many solutions. However, these solutions all correspond to a single foot center force, torque and joint reference torques. The reference torque solution will allow for only one solution to the optimization. Irrespective of whether the solutions adhere to the compatibility relations, the optimization scheme selects one at random. Regardless of the solution selected, the optimization process ends with the same joint torque reference. The resulting contact force, which is likely to deviate from the reference contact force after applying this joint torque, is one of the viable set of solutions for the optimization strategy. The objective is to make sure that the contact forces meet their requirements by giving particular information, as following the reference contact forces is not practical. With reference reaction forces on joints computed, $\tau_{ref} = \mathbf{u}_{E_{3ref}} + \mathbf{b}'_3$ will track the reference reaction forces at steady state, considering the leg dynamics

$$\mathbf{H}'_{33}\ddot{\theta} + \begin{bmatrix} \mathbf{H}'_{31} & \mathbf{H}'_{32} \end{bmatrix} \begin{pmatrix} \dot{\mathbf{v}}_B \\ \dot{\mathbf{w}}_B \end{pmatrix} + \mathbf{b}'_3 + \mathbf{u}_{E_3} = \tau \tag{4.10}$$

This scheme is used in this thesis to provide support for the robot body when pushing the trolley with hands. The hand contact force references are fed to the reactive force scheme as force reference for the robot body and the corresponding leg joint torques are added to the joint torques due to walking or standing controller.

5. ZMP BASED WALKING REFERENCE GENERATION

Chapter 4 covered the topic of a feedforward body control system that uses response forces on the supporting legs. Although it is not the primary control mechanism employed when walking, the reactive force control scheme can be utilized to keep one's balance when manipulating things or exerting force on them. The biped robot in this thesis pushes a trolley that is set apart from it. The robot must approach the trolley on foot before pushing it. Pushing stops once the trolley has moved a predetermined distance. The walk continues until the hands make touch with the trolley after the hands have returned to their initial position. As a result, the robot moves in two phases: walking and pushing.

The motion of the robot starts with a walk towards the trolley that is placed away from the robot in x-direction. The hands are positioned in front of the robot to make sure that the initial contact will be made with the hands. The walk from the starting position to the trolley in the beginning and the walks in between the pushes are realized by a ZMP based reference generation method. This section discusses about the ZMP based reference generation proposed in (Erbatur and Kurt 2009). This method is used in this thesis.

Figure 5. 1 displays a kinematic arrangement of the legs and body of a biped.

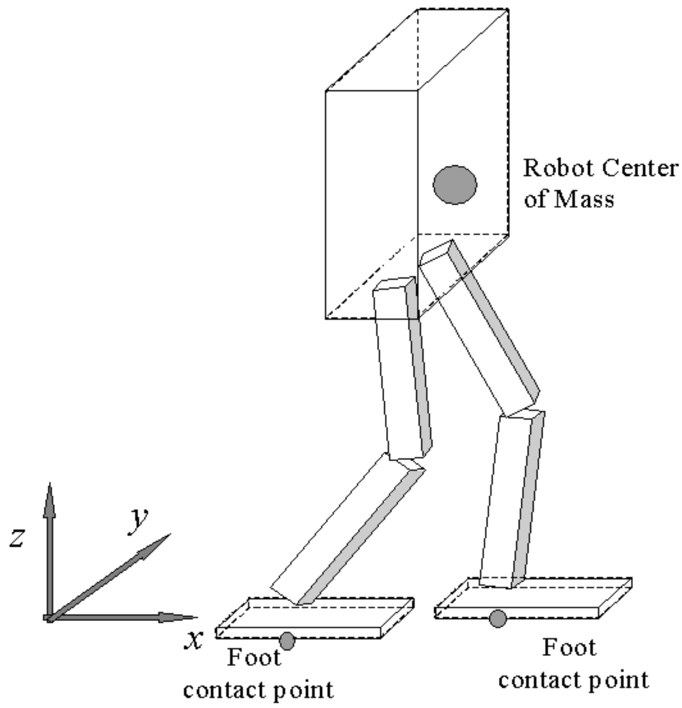

Figure 5. 1 Biped robot kinematic arrangement

A linear inverted pendulum model is a better fit for reference generation and controller design than intricate complete dynamics models.. The robot's body, or trunk, is represented by a point mass that corresponds to the CoM of the robot. Through the use of a massless rod, the point mass is connected to a stable ground contact point. An idealized representation of a supporting leg is the rod. It is also assumed that the swing leg has no mass. We obtain a linear system that is decoupled in both directions, assuming that the robot CoM has a fixed height. The representation of a Linear Inverted Pendulum Model is given in Figure 5. 2. $c = (c_x \quad c_y \quad c_z)^T$ denotes the coordinates the pointless mass in the figure 5.2.

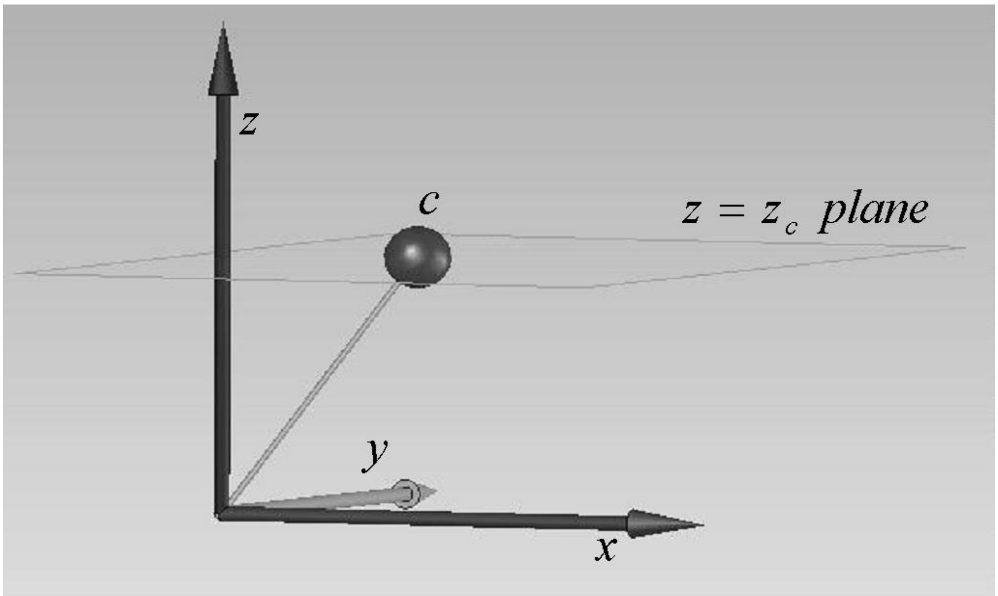

Figure 5. 2 Linear Inverted Pendulum Model

The point where the net torque on $x - y$ axis is zero is defined as the ZMP. (Choi, You & Oh, 2004) ZMP and CoM can be related by the (5.1) and (5.2) according to the linear inverted pendulum model shown in. The ZMP coordinates are p_x, p_y, z_c is the height of the plane were the point mass is constrained and g is the gravity constant.

$$p_x = c_x - \frac{z_c}{g}\ddot{c}_x \tag{5.1}$$

$$p_y = c_y - \frac{z_c}{g}\ddot{c}_y \tag{5.2}$$

According to the ZMP stability criterion, the robot is stable if the defined point is inside the convex hull of the foot-supporting area. With this proposition a reference generation can be implemented. Three possible reference generation techniques are going to be discussed which is proposed in figures 5.3, 5.4 and 5.5 where A is the distance between the foot centers in the y direction, B is the step size and T is the half of a walking period.

The method shown in Figure 5. 3 is based on incrementally increasing the ZMP in x -direction. The ZMP is located on the middle point of the supporting foot sole. This step-like increase in p_x^{ref} results in a non-natural walk. To increase the naturalness of the walk the method in Figure 5. 4 proposes the ZMP to move forward under the foot sole during the single-support phase. The movement of ZMP under the foot sole is denoted by b .With ZMP moving forward under the foot sole, a smoother p_x^{ref} was proposed (Erbatur, Kurt, 2009). Hence, the walk has a more natural characteristic. Still, there's potential for improvement in terms of a more organic gait. A novel technique for inserting a double support phase in between swing phases was presented in Figure 5.5a. (Erbatur et al, 2009) The parameter that can be flexibly altered is used to introduce the twofold support phase. A linear interpolation interval is inserted at intervals that are multiples of the half walking time. The durations of the intervals, which represent double support periods, equal. In figures 5.3c and 5.4c, the right swing to left swing does not change abruptly; rather, a more gradual transition is made possible by the double support phase..

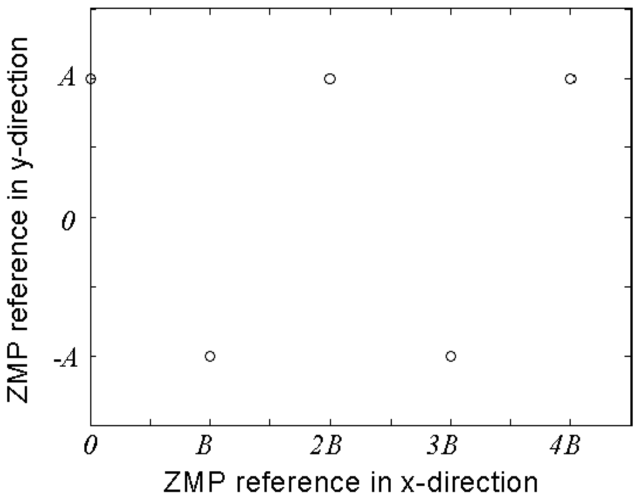

a)

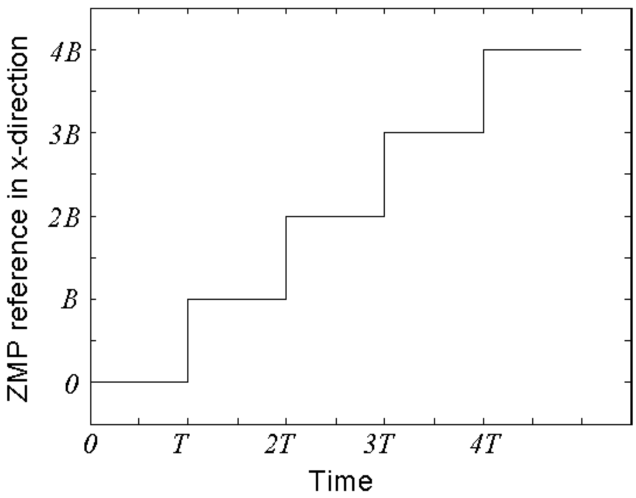

b)

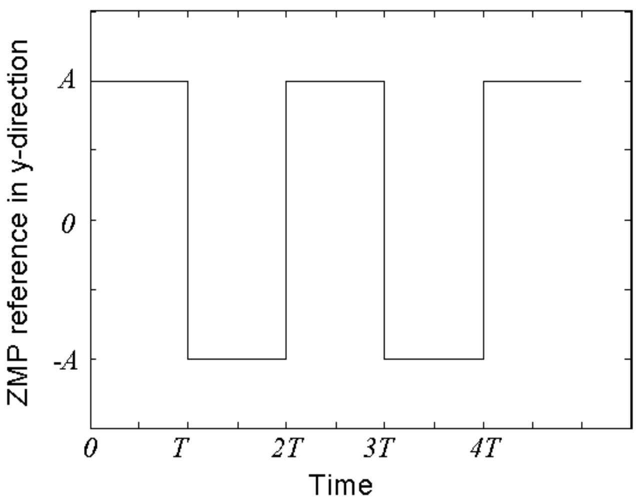

c)

Figure 5. 3 Fixed ZMP references. a) $p_x^{ref} - p_y^{ref}$ *relation on the* $x-y$ *plane b)* p_x^{ref} *, the* x *-axis ZMP c)* p_y^{ref} *, the* y *-axis ZMP reference*

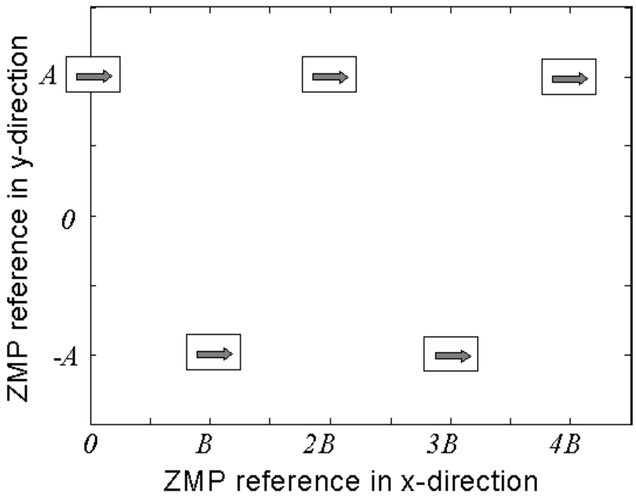

a)

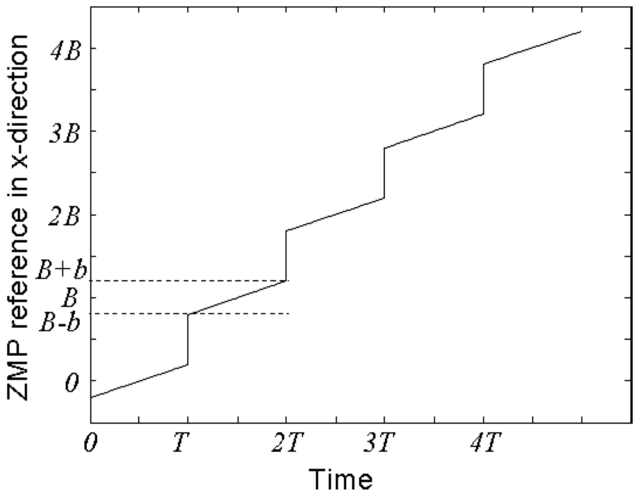

b)

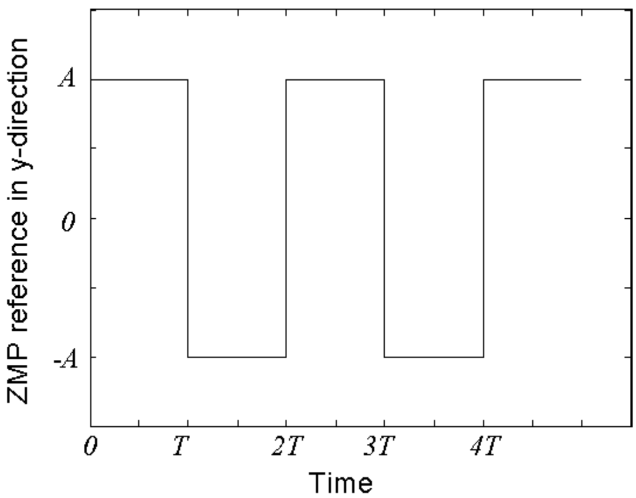

c)

Figure 5. 4 Forward moving ZMP reference a) $p_x^{ref} - p_y^{ref}$ *relation on the* $x-y$ *plane b)* p_x^{ref} *, the* x *-axis ZMP The difference from Figure 5. 3 can be seen c)* p_y^{ref} *, the* y *-axis ZMP reference*

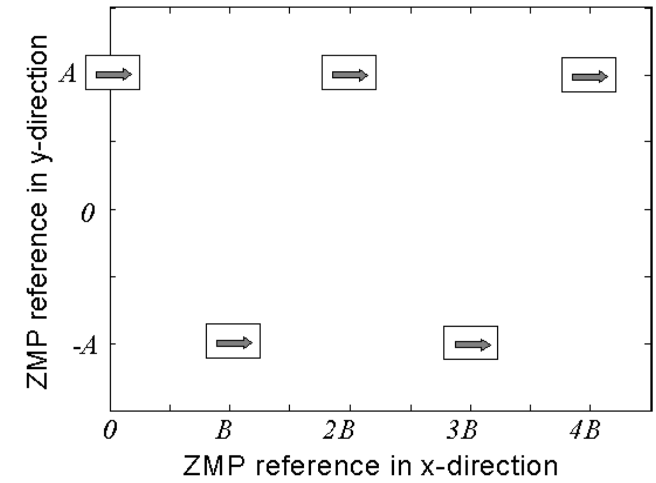

a)

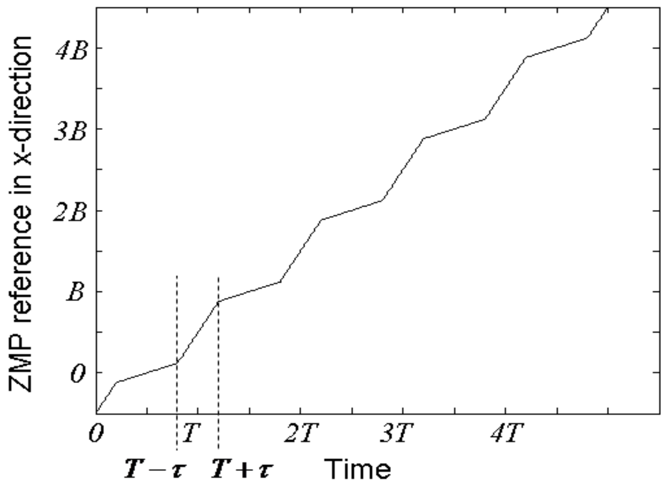

b)

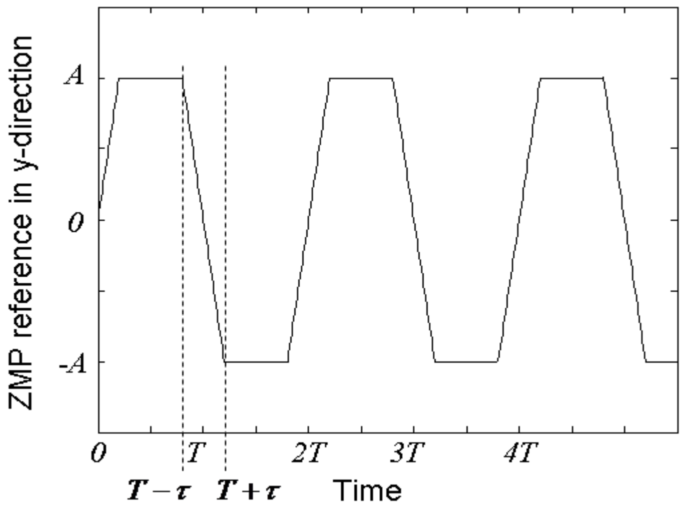

c)

Figure 5. 5 Forward moving ZMP reference with pre-assigned double support phase a) $p_x^{ref} - p_y^{ref}$ relation on the $x-y$ plane b) p_x^{ref} , the x -axis ZMP c) p_y^{ref} , the y -axis ZMP reference

The mathematical description of $p_x^{ref}(t)$ in Figure 5. 5 that relates the step-size and walking period to ZMP with respect to time is given by

$$p_x^{ref} = \frac{B}{T}(t - \frac{T}{2}) + p_x'^{ref} \tag{5.3}$$

$p_x'^{ref}$ is periodic with T and can be formalized by a three-line segments as follows

$$p_x'^{ref} = \begin{cases} \frac{\delta}{\tau} t & \text{if} \quad 0 \le t \le \tau \\ \delta + \frac{-2\delta}{T - 2\tau}(-\tau + t) & \text{if} \quad \tau < t \le T - \tau \\ -\delta - \frac{\delta}{\tau}(T - \tau + t) & \text{if} \quad T - \tau < t \le T \end{cases} \tag{5.4}$$

where

$$\delta = \frac{T - 2\tau}{T}(\frac{B}{2} - b)$$

With the mathematical description of p_x^{ref} is set, one can observe that it is a combination of periodic and non-periodic terms. The $p_x'^{ref}$ term is periodic with T and the $\frac{B}{T}(t - \frac{T}{2})$ section is non-periodic. The magnitude of peak difference between these two terms actually refers to δ which is visualized by Figure 5. 6

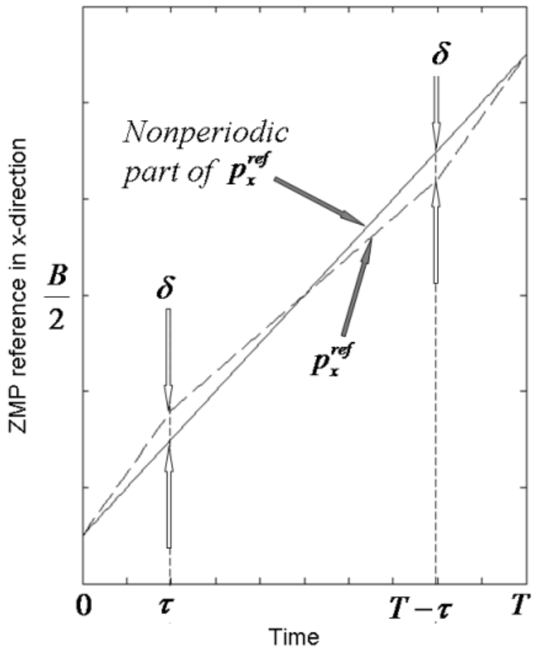

Figure 5. 6 Visualization of δ

The ZMP y-reference changes as well with the proposed method in Figure 5. 5. From a geometrical standpoint it can be formulated with $u(\cdot)$ used as a unit step-function. Note that (5.5) to obtain $p_y^{ref}(t)$ is periodic with $2T$.

$$p_y^{ref} = \sum_{k=1}^{\infty} \mathrm{A}(-1)^k \left[\frac{2}{2\tau}(t-kT)\left[u(t-(kT-\tau))-u(t-(kT+\tau))\right] + \left[u(t-(kT+\tau))-u(t-(kT+T-\tau))\right] \right] \tag{5.5}$$

This thesis computes the CoM reference trajectory using ZMP reference trajectories and a straight walk ZMP reference, utilizing a Fourier series approximation approach. $p_x^{ref}(t)$ and $p_y^{ref}(t)$. (Erbatur et al. 2009)

Let $\omega_n \equiv \sqrt{g/z_c}$ and rewrite (5.1) and (5.2) as

$$\ddot{c}_x^{ref} = \omega_n^2 c_x^{ref} - \omega_n^2 p_x^{ref} \tag{5.6}$$

$$\ddot{c}_y^{ref} = \omega_n^2 c_y^{ref} - \omega_n^2 p_y^{ref} \tag{5.7}$$

One can assume that $c_y^{ref}(t)$ is a periodic function due to the periodic characteristic of $p_y^{ref}(t)$ presented in (5.5). As a result, Fourier series approximation can be implemented to obtain $c_y^{ref}(t)$.

$$c_y^{ref}(t) = \frac{a_0}{2} + \sum_{k=1}^{\infty} a_k \cos\left(\frac{2\pi kt}{2T}\right) + b_k \sin\left(\frac{2\pi kt}{2T}\right) \tag{5.8}$$

By combining (5.7) and (5.8) $p_y^{ref}(t)$ is derived as

$$p_y^{ref}(t) = c_y^{ref} - \frac{1}{\omega_n^2}\ddot{c}_y^{ref} = \frac{a_0}{2} + \sum_{k=1}^{\infty} a_k \left(1+\frac{\pi^2 k^2}{\omega_n^2 T^2}\right)\cos\left(\frac{2\pi kt}{2T}\right) + b_k\left(1+\frac{\pi^2 k^2}{\omega_n^2 T^2}\right)\sin\left(\frac{2\pi kt}{2T}\right) \tag{5.9}$$

From Figure 5. 5 we can conclude that $p_y^{ref}(t)$ is symmetric around the origin, hence making it an odd function. With this property the coefficients $\frac{a_0}{2}$ and $a_k\left(1+\frac{\pi^2 k^2}{\omega_n^2 T^2}\right)$ shall be zero for all k. With this knowledge (5.9) can be simplified as

$$p_y^{ref}(t) = c_y^{ref} - \frac{1}{\omega_n^2}\ddot{c}_y^{ref} = \sum_{k=1}^{\infty} b_k\left(1+\frac{\pi^2 k^2}{\omega_n^2 T^2}\right)\sin\left(\frac{2\pi kt}{2T}\right) \tag{5.10}$$

Finally, the coefficient $b_k\left(1+\frac{\pi^2 k^2}{\omega_n^2 T^2}\right)$ can be computed by a Fourier integral in (5.11).

$$b_k\left(1+\frac{\pi^2 k^2}{\omega_n^2 T^2}\right) = \frac{2}{2T}\int_0^{2T} p_y^{ref} \sin\left(\frac{2\pi kt}{2T}\right)dt \tag{5.11}$$

After the Fourier integral arithmetic steps have been conducted which is omitted due to space considerations, Fourier coefficient b_k can be obtained to calculate $c_y^{ref}(t)$ as

$$\beta_k = \frac{\omega_n^2 T^2}{\pi^2 k^2 + \omega_n^2 T^2}\frac{2}{\pi k}\left\{ \sigma_1\left[-\tau\cos(\frac{2\pi k\tau}{T}) + \frac{T}{2\pi k}\sin(\frac{2\pi k\tau}{T})\right] + \sigma_2\left[\tau\cos(\frac{2\pi k\tau}{T}) - \frac{T}{2}\left(\cos\left(\frac{2\pi k\tau}{T}\right)\right) - \frac{T}{2\pi k}\sin(\frac{2\pi k\tau}{T})\right]\right\} \tag{5.12}$$

for $k = 1,2,3,\cdots$.

With $c_y^{ref}(t)$ known, the second step is to find a relation between $c_x^{ref}(t)$ and $p_x^{ref}(t)$. However, the same principle where we used a Fourier series approximation is not straight forward due to non-periodic term in $p_x^{ref}(t)$, shown in (5.3). The non-periodic term $\frac{B}{T}(t-\frac{T}{2})$ needs to be handled before $c_x^{ref}(t)$ is approximated via Fourier series. With the same assumption used in $c_y^{ref}(t)$ calculation, $c_x^{ref}(t)$ is going to have a both periodic and non-periodic parts. If we assume that the non-periodic parts of $p_x^{ref}(t)$ and c_x^{ref} are not equal to each other, the difference between the ZMP and CoM in x - direction is going to be non-periodic as well. However, this property should not exist in a continuous walk depicted in Figure 5. 5. Consequently, the assumption of non-periodic parts of $p_x^{ref}(t)$ and c_x^{ref} are equal to each other can be made. Wit these assumptions c_x^{ref} is expressed as.

$$c_x^{ref} = \frac{B}{T}(t-\frac{T}{2}) + \frac{\alpha_0}{2} + \sum_{n=1}^{\infty}\alpha_k\cos(\frac{2\pi nt}{T}) + \beta_k\sin(\frac{2\pi nt}{T}) \tag{5.13}$$

Again, by combing (5.7) and (5.13) the following relation between $p_x^{ref}(t)$ and $c_x^{ref}(t)$ can be written.

$$p_x^{ref}(t) = c_x^{ref} - \frac{1}{\omega_n^2}\ddot{c}_x^{ref} = \frac{B}{T}(t-\frac{T}{2}) + \frac{\alpha_0}{2} + \sum_{n=1}^{\infty}\alpha_k(1+\frac{\pi^2k^2}{\omega_n^2T^2})\cos(\frac{2\pi kt}{T}) + \beta_k(1+\frac{\pi^2k^2}{\omega_n^2T^2})\sin(\frac{2\pi kt}{T}) \tag{5.14}$$

In the previous paragraphs the calculation of Fourier coefficients for $c_y^{ref}(t)$ has been provided. The same steps apply to the $c_x^{ref}(t)$ calculations as well. Therefore, only the coefficient results are provided.

$$\frac{\alpha_0}{2} = 0$$

$$\alpha_k (1 + \frac{\pi^2 k^2}{\omega_n^2 T^2}) = 0$$

$$\begin{aligned}\beta_k = \frac{\omega_n^2 T^2}{\pi^2 k^2 + \omega_n^2 T^2} \frac{2}{\pi k} \Bigg\{ & \sigma_1 \left[-\tau \cos(\frac{2\pi k \tau}{T}) + \frac{T}{2\pi k} \sin(\frac{2\pi k \tau}{T}) \right] \\ & + \sigma_2 \left[\tau \cos(\frac{2\pi k \tau}{T}) - \frac{T}{2} \left(\cos\left(\frac{2\pi k \tau}{T} \right) \right) \right. \\ & \left. - \frac{T}{2\pi k} \sin(\frac{2\pi k \tau}{T}) \right] \Bigg\}\end{aligned} \tag{5.15}$$

For $k = 1, 2, 3 ...$

The curves generated by using the technique discussed above are given in Figure 5. 7. and (5.13) require infinite sums which are approximated by changing the summation from $\sum_{k=1}^{\infty}$ to $\sum_{k=1}^{N=24}$. Also, the following parameters are used : $A = 0.1$ m, $B = 0.1$ m, $b = 0.04$, $T = 1$ s and $\tau = 0.2$ s.

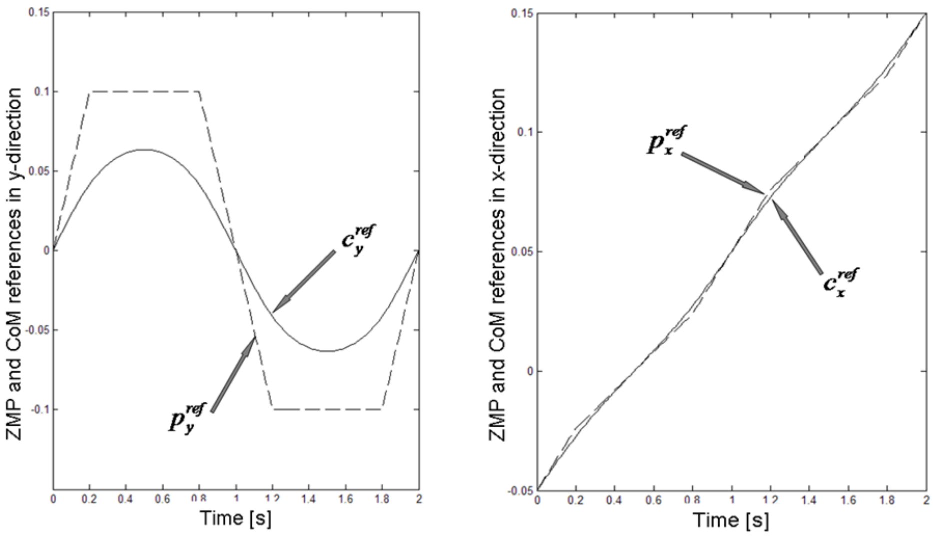

Figure 5. 7 ZMP and CoM references

The foot reference trajectories in x and z directions are employed. Figure 5. 8 displays the mentioned foot reference trajectories.

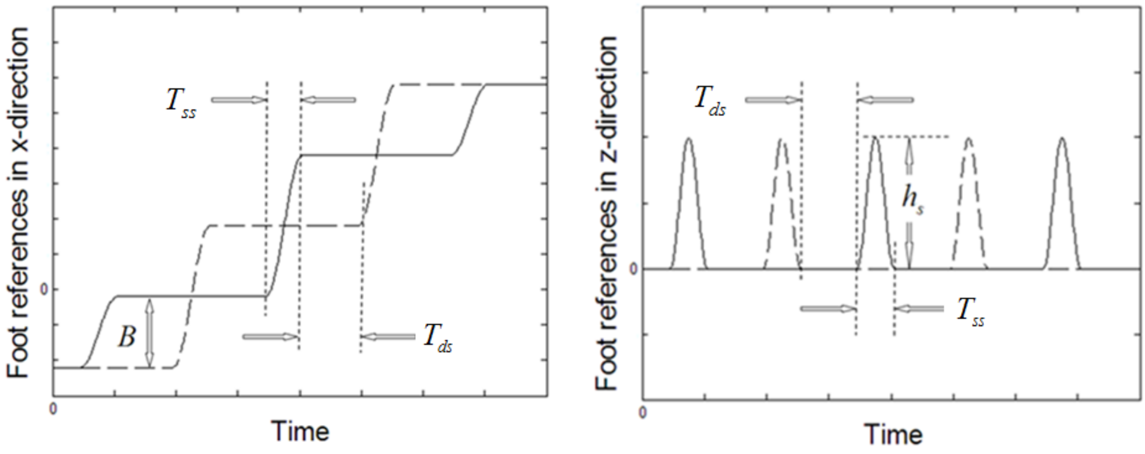

Figure 5. 8 Foot reference trajectories in x and z directions

h_s is the step height parameter. T_{ds} and T_{ss} represent the double and single support periods respectively and B is the step size in this figure.

To determine the reference leg joint positions that link the robot's feet and center of mass, inverse kinematics is solved. The joint references that are produced by inverse kinematics are tracked using independent joint PID position controllers. In addition to the PID controller outputs, the reactive force-based joint torques that were acquired using the method in the preceding section are applied.

6. ARM POSITION-FORCE HYBRID CONTROLLER

After the contact between the robot's end effector and the trolley has been made and the walking has paused, the pushing motion begins. The pushing motion occurs by giving the robot's arms a force reference until a pre-determined displacement is realized with the trolley.

Arm manipulation is realized by a hybrid position-force controller. During the pushing motion the arms are moved in the x-direction. However, the y-z positions need to be retained in their initial contact points which are captured when the hands touch the trolley in the walking stage. Then a PD cartesian position control is applied for both arms to calculate the required force to maintain captured y-z positions shown in (6.1)

$$f_{arm} = K'^{arm}_{p} \begin{pmatrix} e_{pos_{arm}} \\ e_{rot_{arm}} \end{pmatrix} + K'^{arm}_{d} \begin{pmatrix} \dot{e}_{pos_{arm}} \\ \dot{e}_{rot_{arm}} \end{pmatrix} \tag{6.1}$$

Now that y-z positions are retained throughout the pushing motion, the x-direction movement is going to be realized by a reference force on the x-axis. The reference is increasing linearly to a desired force, $f^{desired}_{arm_x}$ to a pre-determined reference. With the reference force in x-direction for arms is known (6.1) is overridden to accommodate all x-y-z reference forces.

$$f_{arm} = \begin{pmatrix} f^{desired}_{arm_x} \\ f_{arm_y} \\ f_{arm_z} \end{pmatrix} \tag{6.2}$$

With the desired forces on all directions the submatrix K_{arm} can link the reference hand contact forces to reaction forces on arms joints.

$$\begin{aligned} \tau^{right}_{arm} &= K^{right}_{arm} f^{right}_{arms} \\ \tau^{left}_{arm} &= K^{left}_{arm} f^{left}_{arms} \end{aligned} \tag{6.3}$$

As a result, the generalized joint torque vector u_{E_3} is formed as

$$u_{E_3} = \begin{pmatrix} u^{legs}_{E_{3ref}} \\ \tau^{right}_{arm} \\ \tau^{left}_{arm} \end{pmatrix} \tag{6.4}$$

After the pushing motion is complete the arms of the robot need to go back to its original position. The home position of the arms allows for a more stable walk and repeatability. With the same position-force hybrid controller, the reference force in the x-direction $f^{desired}_{arm_x}$ is ramped down to 0 N while retaining the y-z captured position.

7. CONTROLLER COORDINATION

2 different control schemes exist depending on the current task of the robot. The chosen control scheme in each phase of the motion is going to be discussed in Chapter 8. In this chapter the details of both possible control schemes are going to be discussed.

Robot's interaction with its environment generates forces and torques on the robot's body and its joints. The external forces generated by the arms and legs are calculated. $u_e = (u_{e_1}, u_{e_2}, u_{e_3})$. The first two sub-vectors, u_{E_1} and u_{E_2}, denotes the net force and torque impacts of the external forces. While most of the time, the external forces are generated by the interaction between the feet of the robot and the ground, pushing motion also contributes to the environmental interaction forces. The final sub-vector u_{E_3} denotes the effect of reaction forces on the joints of the robot. This environment interaction applies for both control schemes.

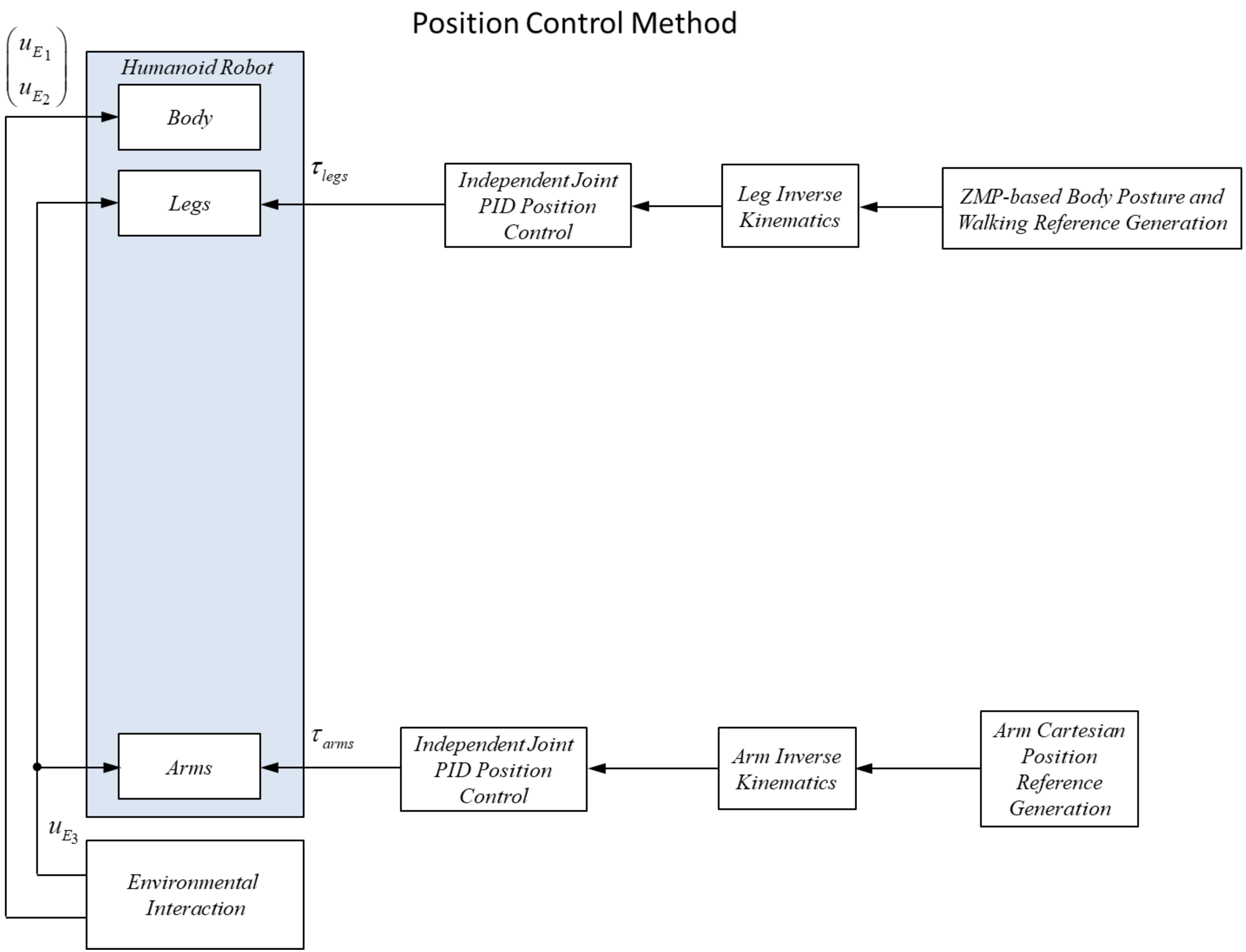

Figure 7. 1 Position control scheme

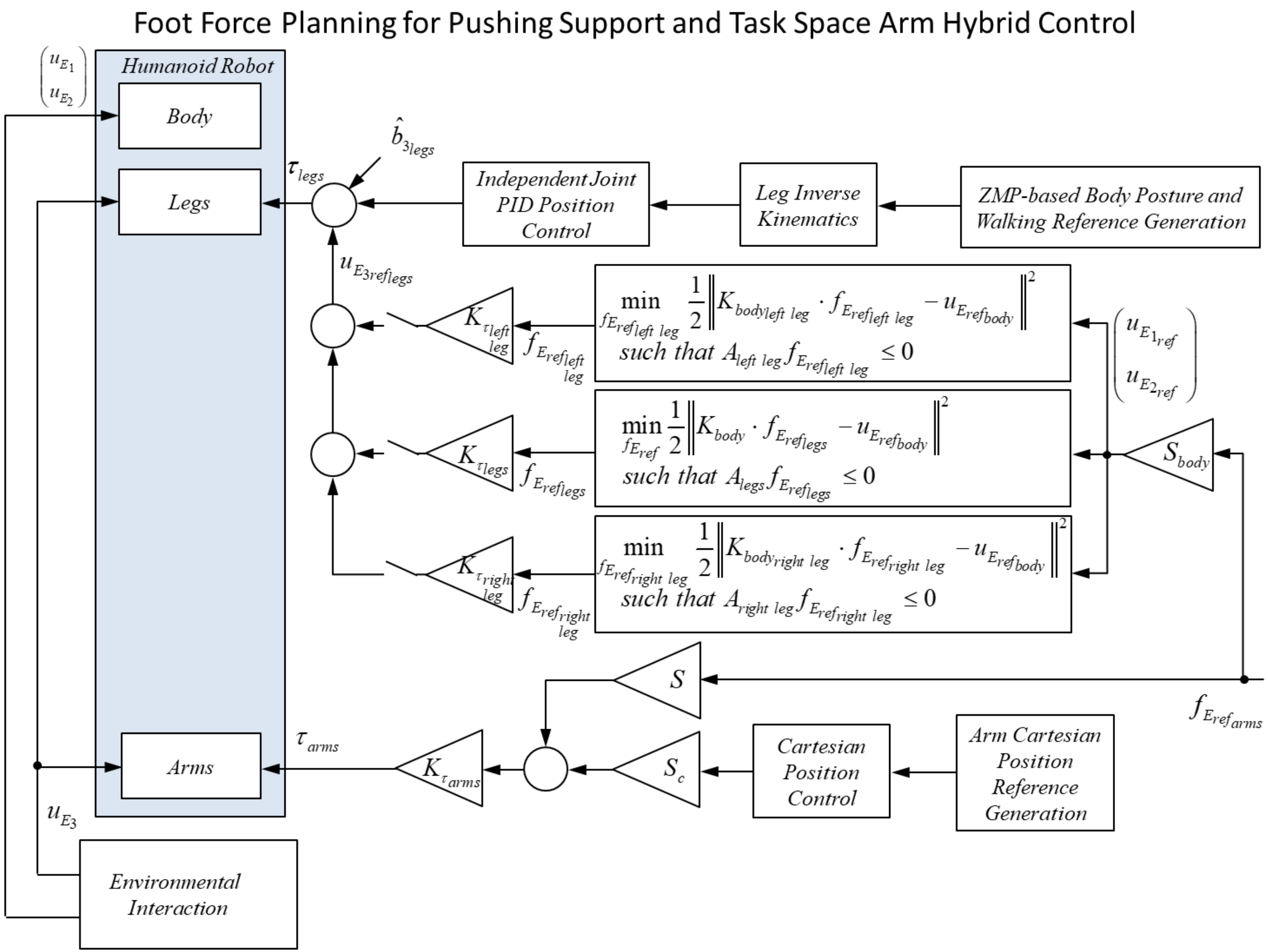

Figure 7. 2 Foot force planning for pushing support and task space arm hybrid controller scheme

The first control scheme is used in situations where arms force reference is non-existent and is subjected to a cartesian position controller. The control scheme is displayed in Figure 7. 1 Position control scheme

A ZMP based body posture and walking reference generation is realized to obtain the position references for leg joints. During reference generation of leg joints, a ZMP based stability criteria is utilized as previously discussed in Chapter 5. The position reference generated for legs is going to depend on the phase of the motion. The reference can either allow for the robot the walk to a certain direction or maintain its position and posture.

The walking position reference is than solved by the leg inverse kinematics to calculate the reference joint torques for the legs. A PID controller was utilized to realize the joint torque references obtained by the position error of the which acts on every joint independently.

In this control scheme arms are also subjected to a cartesian position controller. The generated reference is going to aim to keep the arms in the same position with respect to the robot's coordinate frame. As a result, either in walking or standing, the arm's position and posture with respect to the body is not going to change. The generated reference will be solved by the arms inverse dynamics to generate position a position reference for the PID controller. The PID controller than utilizes the current state and the reference position to generate a reference torque for each joint.

The second control scheme that is used in this controller is provided in Figure 7. 2. The environmental interaction handling, ZMP based body posture and walking reference generation, calculation of independent joint torques from the ZMP based reference generation remains the same with control scheme 1 in Figure 7. 1. However, a new hybrid position-force controller has been introduced to account for pushing motion and an addition to the leg joint torques has been made to further increase stability by using the force reference coming from the hands.

The pushing motion of the robot's arms exert a force to the environment which also effects the body and the stability of the robot. This effect is compensated to enhance the stability by creating a support for pushing. By taking hand force reference into consideration a reference force is generated for the legs. The reference force is than converted to joint angles by using the method discussed in Chapter 4. The calculated reference torque joints to compensate for the arm's exerting force is than added to the reference joint torques obtained through the ZMP based body posture and walking reference generation. Note that the generated reference for pushing support is going to depend on the robot's foot support region as depicted in Figure 7. 2. The controller handles if the robot starts on during single support phase with right or left leg in contact with the ground or double support phase by choosing the suitable constraint matrix, A, and transformation matrix K.

The pushing motion is realized by a hybrid force-position controller for the arms. This controller uses a force reference for its $x-$direction and a cartesian position PID controller for the $y-z$

directions. By doing so, the positions in $y-z$ can be maintained while the arms push forward with a force reference which sets the exerted force magnitude. Due to arms force reference being used for supporting the push, the exerted force through the arms will not disrupt the robot's balance if properly tuned.

8. SIMULATION RESULTS

This thesis utilizes an OpenGL based simulation environment to animate the robot's movements and its interaction with the environment. The references trajectories that the animation uses are obtained by a simulation runs on Simulink with a 5ms cycle time. The controller that has been designed for this thesis is implemented on Simulink. The controller benefits from a state machine like system to allow for phase transitions and easy control method selection. The scheme of the phase transition controller is provided in Figure 8. 1.

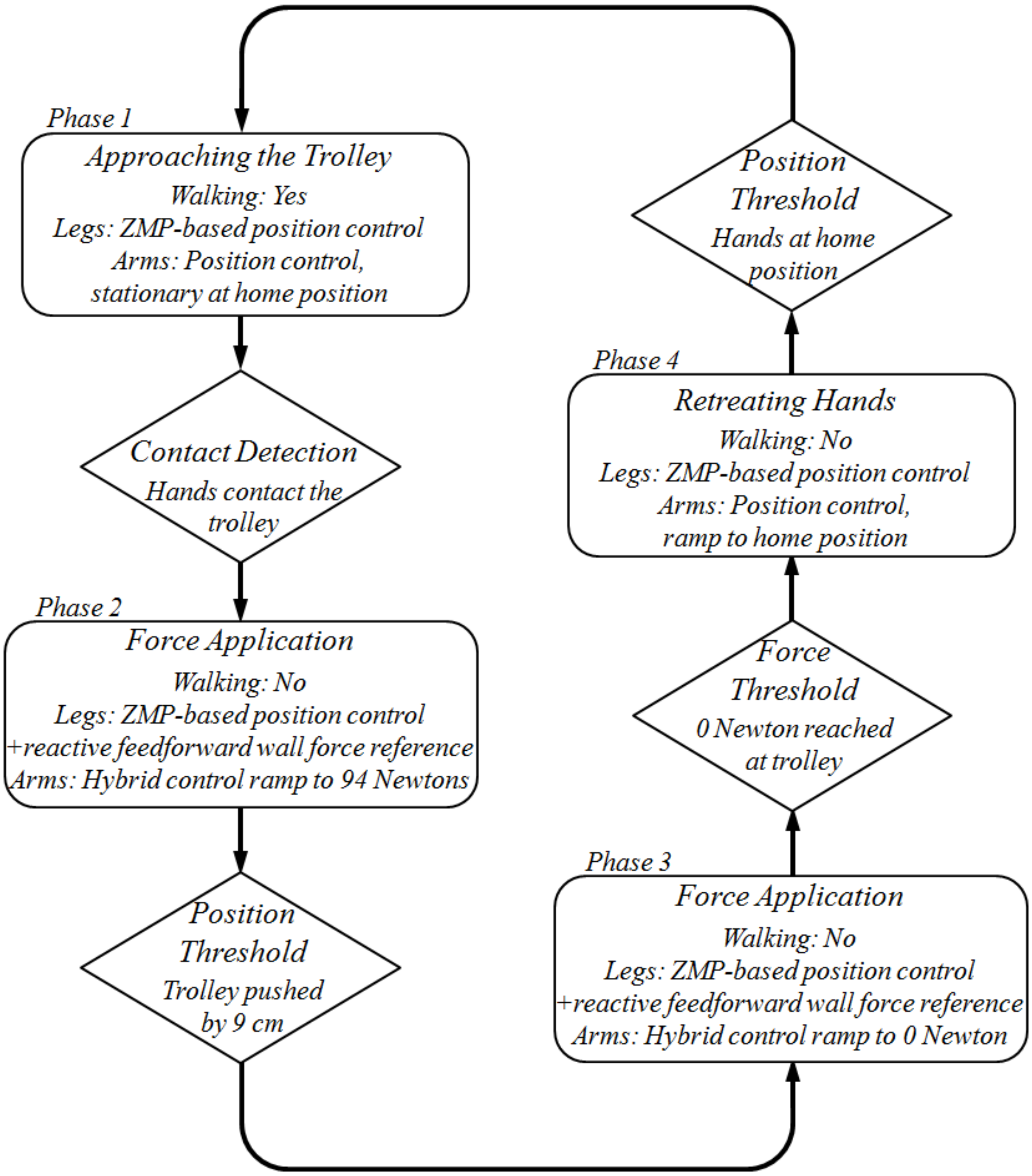

Figure 8. 1 Phase Transition Scheme

This section discusses about the simulation results in a structured way that is divided by the different phases described above. Each phase has its own controller type chosen for both legs and arms as well as a transition condition to the next phase. Due to the cyclic nature of the movement covered in this thesis, the scheme described above is executed a cyclic manner.

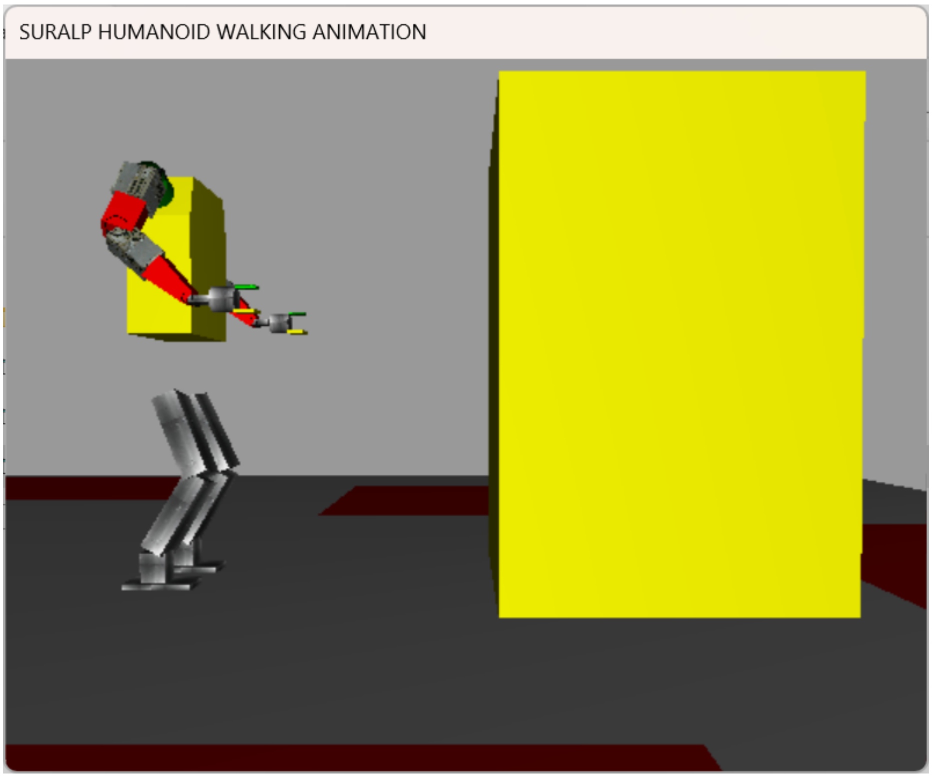

Figure 8. 2 Screenshot of the animation at starting position.

When the simulation starts at $t = 0$ moment the robot is placed 1140mm away from the trolley depicted in Figure 8. 2. The walking begins with the simulation and so does *phase 1*. A ZMP based cartesian position controller is implemented for the walking motion. ZMP based reference generation was discussed in Chapter 5. The reference trajectory is generated by the mentioned controller and executes for movement towards the trolley, which in this case corresponds to the x - direction. A screenshot of the robot during its walk is provided with. Also, arms are subjected to a position controller as well. The position controller has a reference to keep the robot's hand in a steady position which is referred as the home position of the robot. By figures 8.2 and 8.3 one can observe that the arms position and orientation in the robot's reference frame is maintained. The arm's home position during walking also contributes to the stability during its walk. The walk continues until a contact has been detected with the trolley and the hands. This contact triggers to robot continue with its next phase, which is pushing.

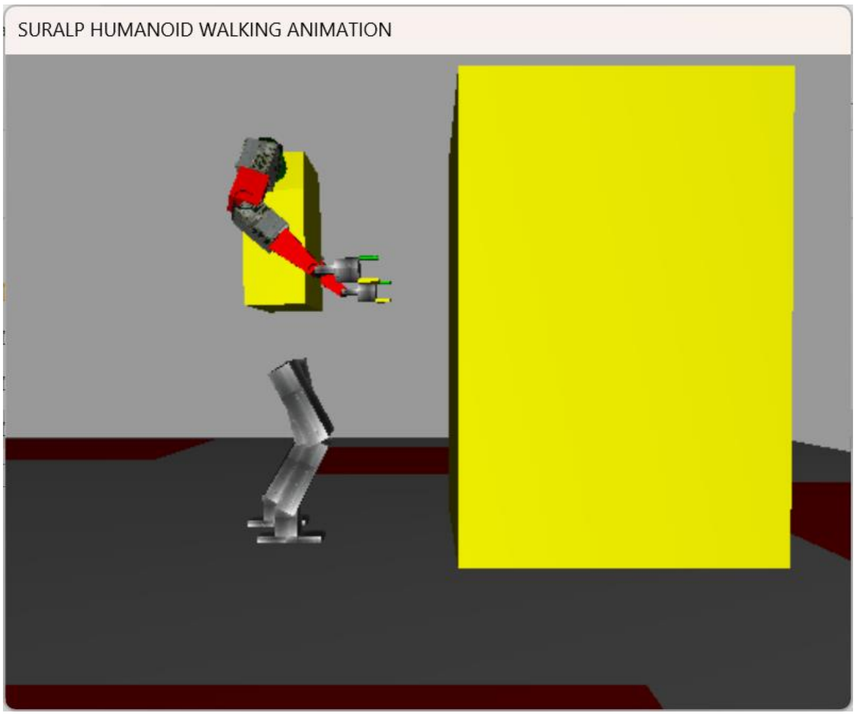

Figure 8. 3 Screenshot of the animation during the 1st walking phase

As soon as the hands make contact with the trolley, the pushing phase begins with *phase 2*, pausing the walk. The point where a contact has been detected is demonstrated in Figure 8. 4. In the image the parts of the hands are positioned inside the trolley. Due to the spring-damping contact model that was used, contact detection occurs when some part of the hands exceeds the trolley's boundaries in the animation.

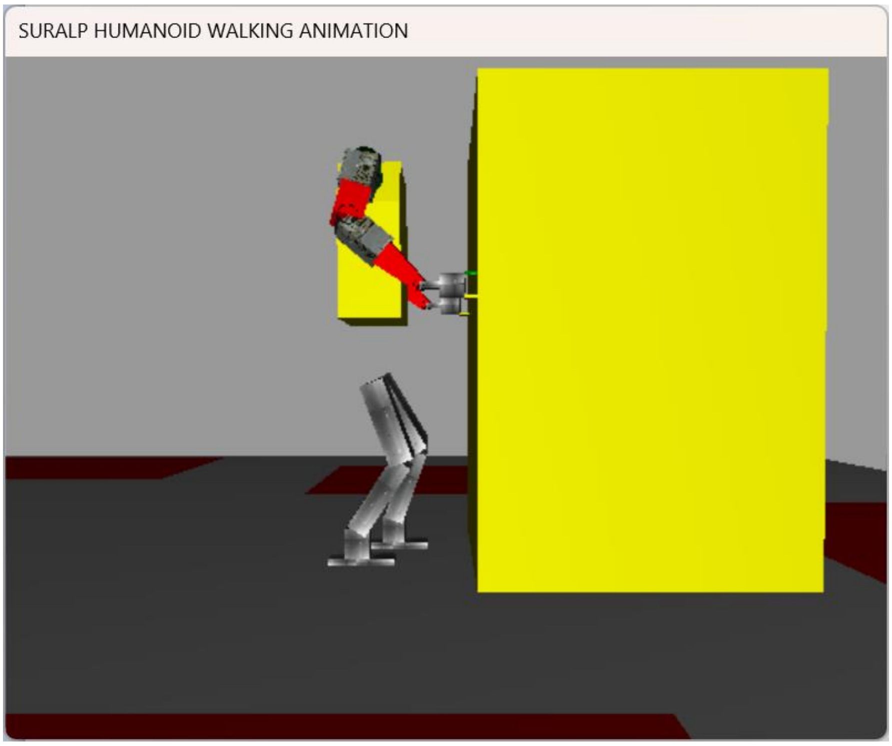

Figure 8. 4 Screenshot of the animation at the moment when a contact is detected

With the contact, the $y - z$ positions of the hands are captured. The captured positions are used to provide an error for the PD controller which receives a position error input and outputs a reference force. The other part of the hybrid position controller is obtained by the force reference in $x-$ direction. The reference trajectory is generated by linearly ramping the force reference to 86N. The force reference in $x-$ direction is combined with the outputs of PD controllers for $y - z$ directions to create a force reference trajectory for arms. By these references the arm hybrid position controller exerts force on the x axis while maintaining the captured positions for $y - z$ axis.

Figure 8. 5 displays the robot's posture and trolley's location close to the end of robot's pushing motion. One can observe by difference between arm positions in figures 8.4 and 8.5, that the trolley has been pushed by the hands. Also, the captured $y - z$ points have been maintained during pushing.

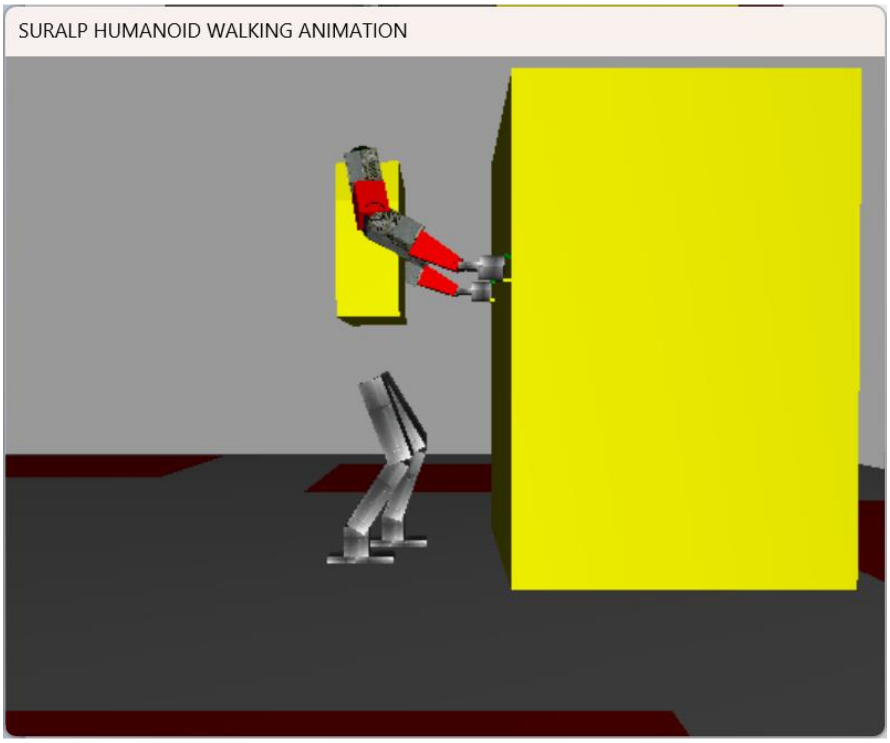

Figure 8. 5 Screenshot of the animation during the pushing phase

During *phase 2*, legs are still in ZMP based position control. However, the reference position does not change, and robot stays in its first contact position The first contact can be made both in single and double support phases depending on the step size, the distance between the trolley and the robot and the position of the robot when it first starts the walk. If the contact was made during a double support phase the body posture is maintained. However, if single support- phase initiates the contact, the leg that is not touching the ground freely falls to the ground by gravity and the body posture is frozen for the pushing movement. Based on the support phase at the time which the contact was made, suitable transformation matrices are selected to execute the simulation. Each support phase, single or double, is handled differently during the pushing motion.

During any manipulation task that is realized by the upper body poses a challenge on maintaining the stability of the robot. If the exerted force by the arms is enough to shift the ZMP out of the foot supporting region, robot falling over inevitable. Consequently, a reactive feedforward wall reference is implemented to compensate for the external forces described in chapter 4. To ensure further stability during pushing phase, a set of joint torques are calculated to compensate for the exerted force by the hands. The calculated torques are than added to the already existing joint torque reference which is generated by the ZMP based position controller for the legs. By adjusting the torque joint references, additional reactive force is created from the ground, resulting in a more stable pushing motion.

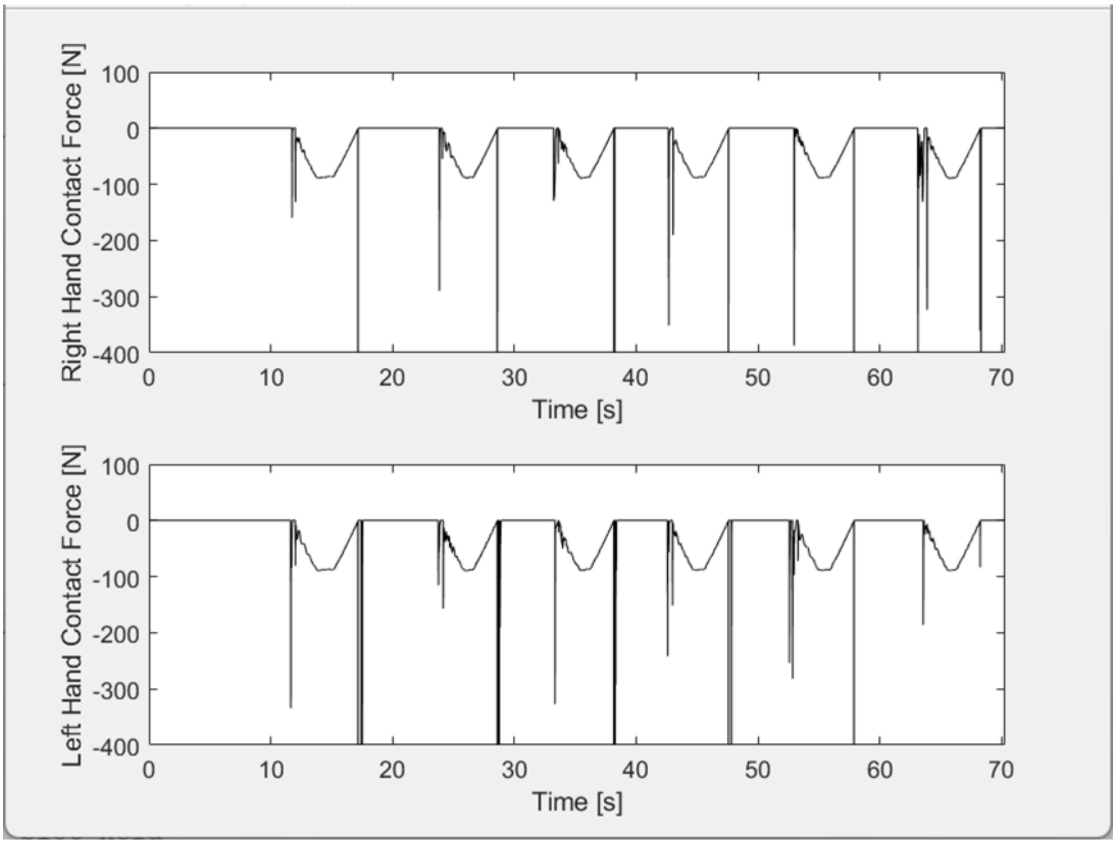

Figure 8. 6 Right- and left-hand contact forces plot

The exerted force plot on the trolley is shown in Figure 8. 6. The plot consists of two subplots for each of the hands that exert force on the trolley with respect time. This plot was generated by calculating the reaction force to the robot's hands, hence the negative sign of the force. A cycle of six walk and push motions were captured for this data. After the 10 second mark the hand's contact forces linearly increases to -86N. After the maximum force is reached the contact force remains as -86N and linearly decreases to 86N. These correspond to *phase 2* and *phase 3* respectively. This cycle is repeated six times in this figure. Spikes can be observed during the initial contact and the moment prior to contact terminating. This can be explained by the wood-pecker effect.

The pushing motion terminates when the trolley has a displacement of 90mm. After the pushing motion *phase 3* begins. This is the phase where the force reference trajectory in $x-$direction is ramped to 0N from 86N. The decrease in the reference force was realized to address the issue of computational error between the inverse kinematics and Jacobian transpose methods for joint torques. The position controller uses inverse kinematics to solve for joint torques during walking and Jacobian transpose is used to generate a reference for hybrid position controller mode for pushing. In between these phase transitions the difference between calculated joint torques can result in instantaneous movements for the arm which may cause the robot to lose its balance. The same ZMP based position controller with a reactive feedforward wall reference is utilized to maintain the robot's position. As the arm reference force decreases, the reactive force and the compensation for the exerted hand forces decrease as well. Hence, *phase 3* is utilized to decrease the reference force to 0N and smoothly transition from pushing to walking.

Figure 8. 7 Screenshots of the animation during after the hand retreating phase.

After the arm reference force has decreased to 0N, *phase 4* begins. This phase is to restore the home position of arms, preparing the robot for its next cycle. Now that the reference force for hands is 0Nm, it is safe to transition into a position controller where the arms going to be retreated to its home position. The position of the robot retreats its arms is shown in Figure 8. 7. With this phase, the reactive feedforward wall reference generation is terminated and the robot transitions into the position controller where the reference remains the same while retreating the hands.

When the arms reach the home position, *phase 1* begins again with the walk and whole cycle is repeated. However, there exists a difference between the first cycle and all the others, which is the travel distance during walking. Since the initial position of the robot and the trolley is much further away than any other cycle, the walking is much more important during the first *phase 1*. The difference between the walking distance can be observed by comparing figures8.2 and 8.7 shows the end of walking and pushing phases during the 2nd cycle. Figure 8. 9 displays the pushing motion during 2nd cycle.

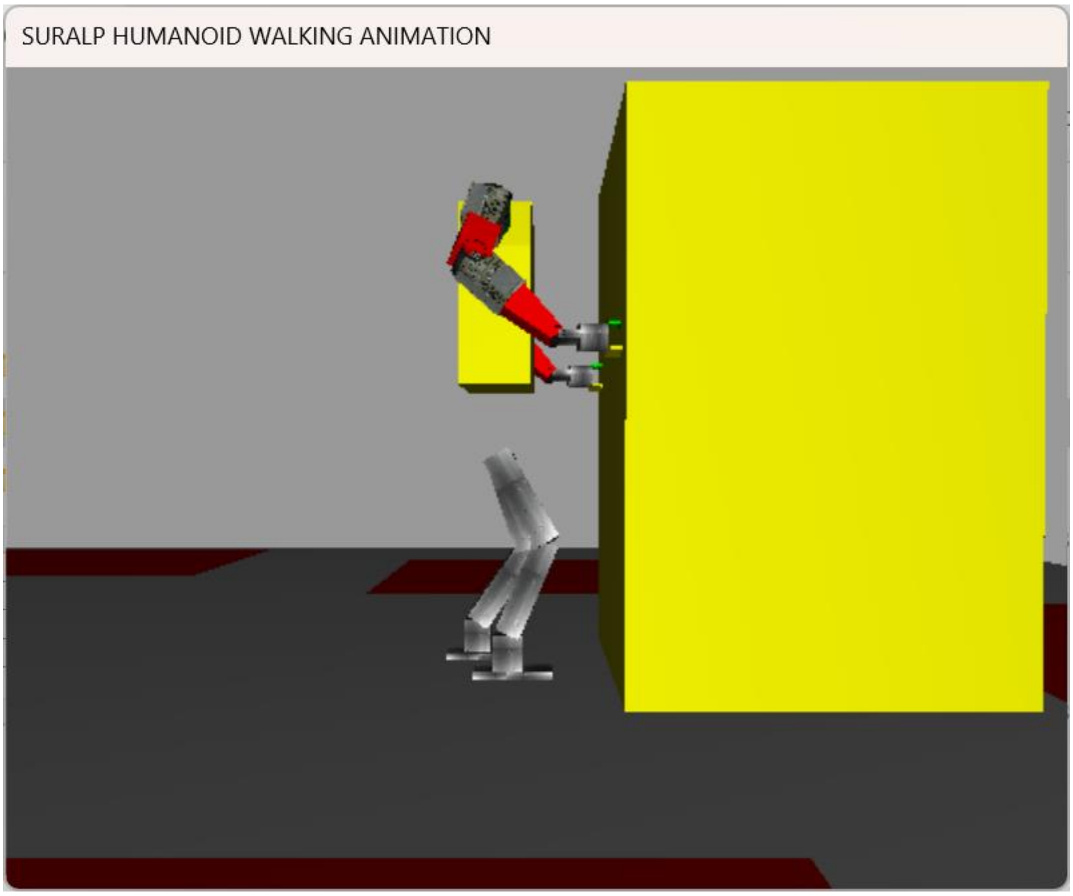

Figure 8. 8 Screenshots of the animation during 2nd cycle contact detecting phase.

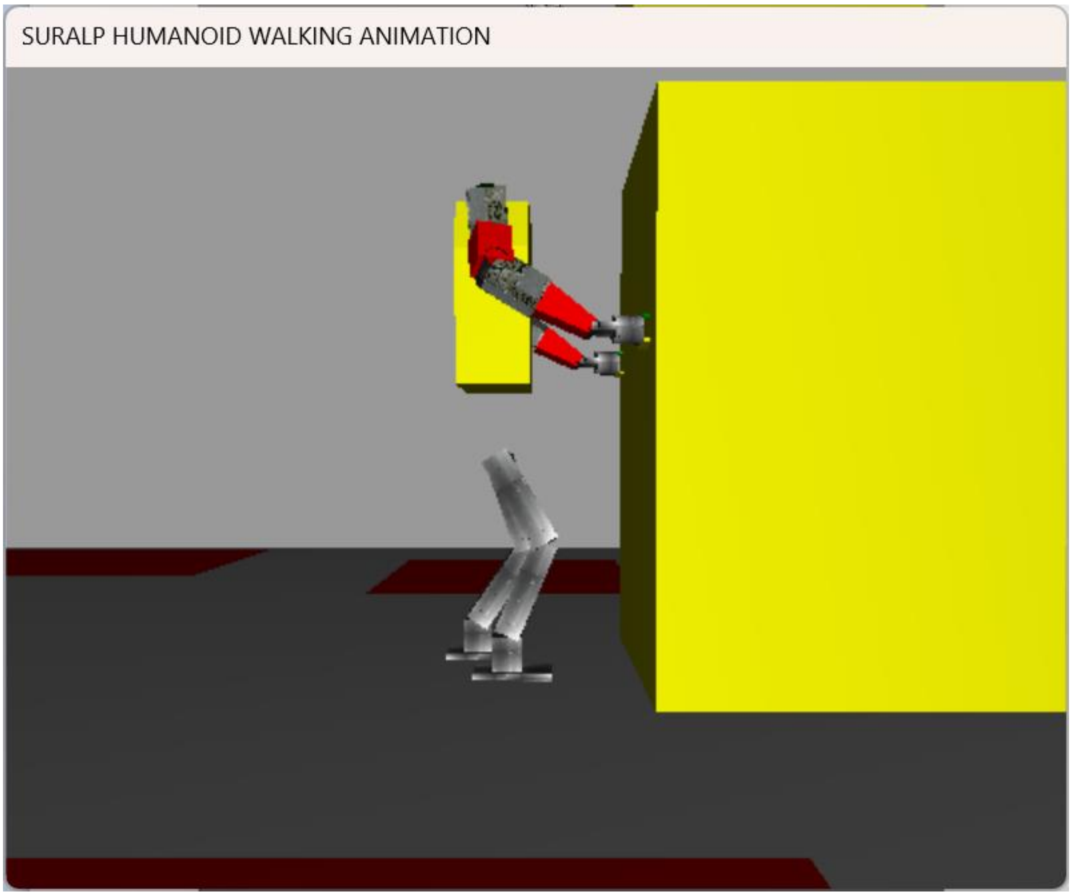

Figure 8. 9 Screenshots of the animation during 2nd cycle pushing phase.

The trolley and the robot’s body positions during the simulation are plotted in Figure 8. 10. The robot and the trolley begin with a distance over 1m. The walking and the pushing phases are executed, creating a small distance between them. Then the robot walks again to the trolley, makes contact with and the pushes again. The effect of all these steps and the phases described above are observable in the figure. The robot was able to move the trolley around 540mm with 6 cycles in around 70 seconds.

There exists a spike in the trolley position after each pushing motion ends. The linear increase of the trolley position terminates after the displacement has reached 90mm. However, after a certain amount of time the trolley position has an instantaneous increase even though it is relatively very small. This is caused by the following phenomena: When the pushing motion terminates and the robot’s arms come to a sudden stop, a sway occurs with the arms of the robot, resulting in a very small amount of push.

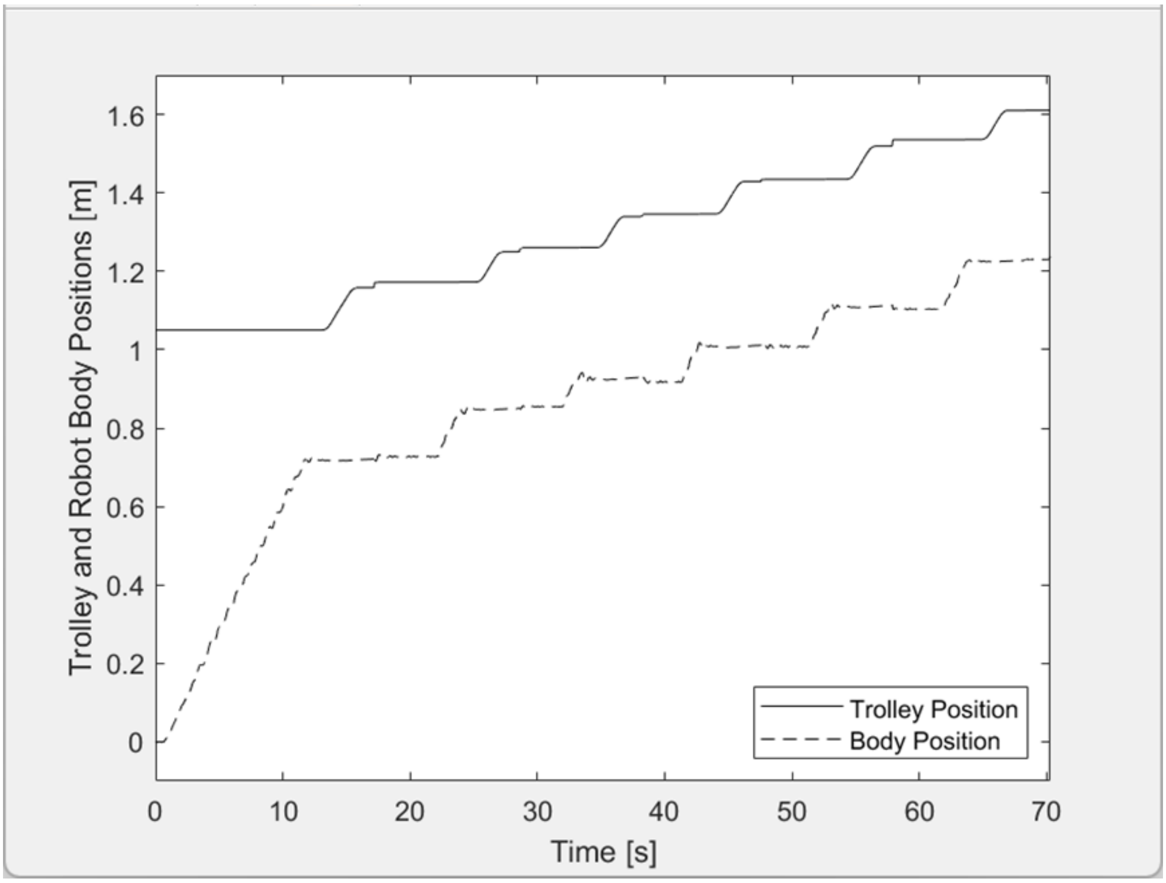

Figure 8. 10 Trolley and body position plot

9. CONCLUSION

Pushing an object by hands and changing its position is a humanoid robot task which can find application in daily life and industrial setting human-robot coexistence scenarios. Pushing a trolley is a typical operation. This thesis proposes a reference generation, control and coordination technique to move a trolley by hand contact and bipedal walk.

Being in force interaction with the environment can be potentially dangerous for a legged robot, even more so when compared with industrial manipulators and wheeled or tracked mobile robots. This is since the legged robot is prone to losing balance and fall when faced with disturbance forces.The thesis takes an experimental approach facilitated by the 3D dynamics simulation environment of the robot SURALP designed at Sabancı University. A repetitive algorithm comprising of motion phases described by walking and hand motion template is developed. When one phase of pushing motion was successfuly designed the next phase was studied and tested.

The sequence of motion starts with a position controlled walk towards the stationary trolley. Hand contact triggers the next phase in which walking pauses and hands push the trolley under hybrid position-force control. This pushing phase also benefits from ground contact forces computed via an optimization technique. After a certain amount of dislocation of the trolley by the hand push, hands retreat and walking resumes to generate the next hand contact. This cyclic motion is shown to move the trolley to any desired distance.

The presented method has the potential of being employed not just as a technique for moving of trolleys but also as an approach for implementing assembly tasks in which relatively large building blocks are positioned by hands with the assistance of the walk.

It should be mentioned that the developed pushing algorithm is only one approach out of uncountably many styles of pushing a trolley or a cart. Moving an object on wheels or tracks without losing hand contact throughout the walk would be a natural extension of the proposed thesis. Also, pushing a trolley on a two-dimensional reference trajectory is considered as a future work.

10. BIBLIOGRAPHY

Akhtaruzzaman, Md. (2010). Advancement of Android and Contribution of Various Countries in the Research and Development of the Humanoid Platform. cscjournals.org.

Albert, Amos & Gerth, Wilfried. (2003). Analytic Path Planning Algorithms for Bipedal Robots without a Trunk. Journal of Intelligent and Robotic Systems. 36. 109-127. 10.1023/A:1022600522613.

ARCH2O HRP-5P, 2024; https://www.arch2o.com/hrp-5p-humanoid-robot-that-will-help-you-remodel/

Azevedo-Coste, Christine & Poignet, Philippe & Espiau, Bernard. (2002). Moving Horizon Control for Biped Robots Without Reference Trajectory. Proceedings - IEEE International Conference on Robotics and Automation. 3. 2762 - 2767. 10.1109/ROBOT.2002.1013650.

Boston Dynamics, 2024; https://bostondynamics.com/atlas/

Cheng, G., Hyon, S.-h., Morimoto, J., Ude, A., Colvin, G., Scroggin, W., & Jacobsen,S. C. (2006). CB: A Humanoid Research Platform for Exploring NeuroScience.In 2006 6th IEEE-RAS International Conference on Humanoid Robots, (pp. 182–187). ISSN: 2164-0580.

Chevallereau, C., Bessonnet, G., Abba, G., & Aoustin, Y. (Eds.). (2009). Kinematic and Dynamic Models for Walking, (pp. 1–126). John Wiley Sons, Ltd.

Choi, Youngjin & You, Bum-Jae & Oh, Sang-Rok. (2004). On the stability of indirect ZMP controller for biped robot systems. 2. 1966 - 1971 vol.2. 10.1109/IROS.2004.1389686.

Cholewiak, Steven A., Fleming Roland W., Singh, Manish; Perception of physical stability and center of mass of 3-D objects. Journal of Vision 2015;15(2):13.

Erbatur, K. And Kurt, O. "Natural ZMP Trajectories for Biped Robot Reference Generation," in IEEE Transactions on Industrial Electronics, vol. 56, no. 3, pp. 835-845, March 2009, doi: 10.1109/TIE.2008.2005150.

Erbatur, Kemalettin & Koca, Özer & Yilmaz, Metin & Seven, Utku. (2009). ZMP Based Reference Generation for Biped Walking Robots. 58.

Forbes Robotics ASIMO, 2022; https://www.forbes.com/sites/peterlyon/2022/03/28/hondas-globetrotting-pint-sized-robot-asimo-to-retire/

Galdeano, David & Chemori, Ahmed & Krut, Sébastien & Fraisse, Philippe. (2016). Optimal Pattern Generator for Dynamic Walking in humanoid Robotics.

H. Hirukawa et al., "A universal stability criterion of the foot contact of legged robots - adios ZMP," Proceedings 2006 IEEE International Conference on Robotics and Automation, 2006. ICRA 2006., Orlando, FL, USA, 2006, pp. 1976-1983, doi: 10.1109/ROBOT.2006.1641995.

Harada, Kensuke & Kajita, Shuuji & Kanehiro, Fumio & Fujiwara, Kiyoshi & Kaneko, Kenji & Yokoi, Kazuhito & Hirukawa, Hirohisa. (2007). Real-Time Planning of Humanoid Robot's Gait for Force-Controlled Manipulation. Mechatronics, IEEE/ASME Transactions on. 12. 53 - 62. 10.1109/TMECH.2006.886254.

Harada, Kensuke & Kajita, Shuuji & Kaneko, K. & Hirukawa, H.. (2003). Pushing manipulation by humanoid considering two-kinds of ZMPs. 2. 1627 - 1632 vol.2. 10.1109/ROBOT.2003.1241827.

Harada, Kensuke & Kajita, Shuuji & Kaneko, Kenji & Hirukawa, Hirohisa. (2006). Dynamics and balance of a humanoid robot during manipulation tasks. Robotics, IEEE Transactions on. 22. 568 - 575. 10.1109/TRO.2006.870649.

Hawley, Louis & Suleiman, Wael. (2017). Control strategy and implementation for a humanoid robot pushing a heavy load on a rolling cart. 4997-5002. 10.1109/IROS.2017.8206382.

Hirose, M., & Ogawa, K. (2007). Honda humanoid robots development. Philosophical transactions. Series A, Mathematical, physical, and engineering sciences, 365(1850), 11–19.

Hirukawa, Hirohisa & Kanehiro, Fumio & Kaneko, Kenji & Kajita, Shuuji & Fujiwara, Kiyoshi & Kawai, Yoshihiro & Tomita, Fumiaki & Hirai, Shigeoki & Tanie, Kazuo & Isozumi, Takakatsu & Akachi, Kazuhiko & Kawasaki, Toshikazu & Ota, Shigehiko & Yokoyama, Kazuhiko & Handa, Hiroyuki & Fukase, Yutaro & Maeda, Jun-ichiro & Nakamura, Yoshihiko & Tachi, Susumu & Inoue, Hirochika. (2004). Humanoid robotics platforms developed in HRP. Robotics and Autonomous Systems. 48. 165-175. 10.1016/j.robot.2004.07.007.

HONDA Robotics ASIMO, 2008; https://web.archive.org/web/20081023205824/http://world.honda.com/ASIMO/technology/

HONDA Robotics, 2008; https://web.archive.org/web/20081204051713/http://world.honda.com/ASIMO/history/history.html

Huang, Q., Yu, Z.G., Chen, X. C., Zhang, W. M., Yang, T. Q.,Liao, W. X., & Ceccarelli, M. (2019). Historical Developments of BHR Humanoid Robots. Advances in Historical Studies, 8,79-90.

Jing, C. & Zheng, J. (2020). Stable walking of biped robot based on center of mass trajectory control. Open Physics, 18(1), 328-337.

Kajita, Shuuji & Kanehiro, Fumio & Kaneko, K. & Fujiwara, Kiyoshi & Harada, Kensuke & Yokoi, Kazuhito & Hirukawa, H.. (2003). Biped walking pattern generation by using preview control of zero-moment point. Proceedings - IEEE International Conference on Robotics and Automation. 2. 1620 - 1626 vol.2. 10.1109/ROBOT.2003.1241826.

Kajita, Shuuji & Kanehiro, Fumio & Kaneko, Kenji & Yokoi, Kazuhito & Hirukawa, Hirohisa. (2001). The 3D linear inverted pendulum model: A simple modeling for a biped walking pattern generation. 1. 239 - 246 vol.1. 10.1109/IROS.2001.973365.

Kajita, Shuuji. (2019). HRP-4 and Other HRP Robots. 10.1007/978-94-007-6046-2_11.

Kaneko, Kenji & Kaminaga, Hiroshi & Sakaguchi, Takeshi & Kajita, Shuuji & Morisawa, Mitsuharu & Kumagai, Iori & Kanehiro, Fumio. (2019). Humanoid Robot HRP-5P: an Electrically Actuated Humanoid Robot with High Power and Wide Range Joints. IEEE Robotics and Automation Letters. PP. 1-1. 10.1109/LRA.2019.2896465.

Lim, H. O., & Takanishi, A. (2007). Biped walking robots created at Waseda University: WL and WABIAN family. Philosophical transactions. Series A, Mathematical, physical, and engineering sciences, 365(1850), 49–64.

Ma, Gan & Gao, Junyao & Yu, Zhangguo & Chen, Xuechao & Huang, Qiang & Liu, Yunhui. (2016). Development of a Socially Interactive System with Whole-Body Movements for BHR-4. International Journal of Social Robotics. 8. 10.1007/s12369-015-0330-y.

Mayne, D.Q. & Rawlings, James & Rao, Christopher & Scokaert, P.. (2000). Constrained Model Predictive Control: Stability and Optimality. Automatica. 36. 789-814. 10.1016/S0005-1098(99)00214-9.

Motoi, Naoki & Ikebe, Motomi & Ohnishi, Kouhei. (2007). Real-Time Gait Planning for Pushing Motion of Humanoid Robot. Industrial Informatics, IEEE Transactions on. 3. 154 - 163. 10.1109/TII.2007.898469.

Navaneeth, M.G., Sudheer, A.P., & Joy, M.L. (2022). Contact Wrench Cone-Based Stable Gait Generation and Contact Slip Estimation of a 12-DoF Biped Robot. Arabian Journal for Science and Engineering, 47, 15947 - 15971.

Nelson, Gabe & Saunders, Aaron & Neville, Neil & Swilling, Ben & Bondaryk, Joe & Billings, Devin & Lee, Chris & Playter, Robert & Raibert, Marc. (2012). PETMAN: A Humanoid Robot for Testing Chemical Protective Clothing. Journal of the Robotics Society of Japan. 30. 372-377. 10.7210/jrsj.30.372.

Nelson, Gabe & Saunders, Aaron & Playter, Robert. (2019). The PETMAN and Atlas Robots at Boston Dynamics. 10.1007/978-94-007-6046-2_15.

Ogura, Yu & Aikawa, Hiroyuki & Shimomura, Kazushi & Kondo, Hideki & Morishima, Akitoshi & Lim, Hun-ok & Takanishi, Atsuo. (2006). Development of a New Humanoid Robot WABIAN-2. 76-81. 10.1109/ROBOT.2006.1641164.

P. -b. Wieber, "Trajectory Free Linear Model Predictive Control for Stable Walking in the Presence of Strong Perturbations," 2006 6th IEEE-RAS International Conference on Humanoid Robots, Genova, Italy, 2006, pp. 137-142, doi: 10.1109/ICHR.2006.321375.

Qiang Huang et al., "A high stability, smooth walking pattern for a biped robot," Proceedings 1999 IEEE International Conference on Robotics and Automation (Cat. No.99CH36288C), Detroit, MI, USA, 1999, pp. 65-71 vol.1, doi: 10.1109/ROBOT.1999.769932.

Rardin, R. L. (2017). Optimization in operations research (Second edition ed.).Boston: Pearson.

S. Feng, X. Xinjilefu, C. G. Atkeson and J. Kim, "Optimization based controller design and implementation for the Atlas robot in the DARPA Robotics Challenge Finals," 2015 IEEE-RAS 15th International Conference on Humanoid Robots (Humanoids), Seoul, Korea (South), 2015, pp. 1028-1035, doi: 10.1109/HUMANOIDS.2015.7363480.

Sakagami, Yoshiaki & Watanabe, Ryujin & Aoyama, Chiaki & Matsunaga, Shinichi & Higaki, Nobuo & FujiMura, Kikuo. (2002). The intelligent ASIMO: System overview and integration. IEEE International Conference on Intelligent Robots and Systems. 3. 2478 - 2483 vol.3. 10.1109/IRDS.2002.1041641.

-Sariyildiz, Emre & Ohnishi, Kouhei. (2013). On the Explicit Robust Force Control via Disturbance Observer. IEEE Transactions on Industrial Electronics. 62. 6551-6556. 10.1109/IECON.2013.6700215.

SARIYILDIZ, EMRE and TEMELTAŞ, HAKAN (2017) "Whole body motion control of humanoid robots using bilateral control," Turkish Journal of Electrical Engineering and Computer Sciences: Vol. 25: No. 2, Article 68.

Shimmyo, Shuhei & Sato, Tomoya & Ohnishi, Kouhei. (2013). Biped Walking Pattern Generation by Using Preview Control Based on Three-Mass Model. Industrial Electronics, IEEE Transactions on. 60. 5137-5147. 10.1109/TIE.2012.2221111.

Stephens, Benjamin & Atkeson, C.G.. (2010). Dynamic Balance Force Control for compliant humanoid robots. 1248 - 1255. 10.1109/IROS.2010.5648837.

Sugahara, Y. & Endo, T. & Lim, H. and Takanishi, A; "Design of a battery-powered multi-purpose bipedal locomotor with parallel mechanism," IEEE/RSJ International Conference on Intelligent Robots and Systems, Lausanne, Switzerland, 2002, pp. 2658-2663 vol.3, doi: 10.1109/IRDS.2002.1041671.

Sugahara, Yusuke & Hosobata, Takuya & Mikuriya, Yutaka & Sunazuka, Hiroyuki & Lim, Hun-ok & Takanishi, Atsuo. (2004). Realization of Dynamic Human-carrying Walking by a Biped Locomotor. 3055-3060. 10.1109/ROBOT.2004.1307526.

Sugano, S. and Kato, I. "WABOT-2: Autonomous robot with dexterous finger-arm--Finger-arm coordination control in keyboard performance," Proceedings. 1987 IEEE International Conference on Robotics and Automation, Raleigh, NC, USA, 1987, pp. 90-97, doi: 10.1109/ROBOT.1987.1088025.

Sugihara, Tomomichi & Morisawa, Mitsuharu. (2020). A survey: dynamics of humanoid robots. Advanced Robotics. 34. 1-15. 10.1080/01691864.2020.1778524.

Takanishi, A. & Lim, Hun-ok, Tsuda, M. and Kato, I. ; "Realization of dynamic biped walking stabilized by trunk motion on a sagittally uneven surface," EEE International Workshop on Intelligent Robots and Systems, Towards a New Frontier of Applications, Ibaraki, Japan, 1990, pp. 323-330 vol.1, doi: 10.1109/IROS.1990.262408.

Takanishi, Atsuo & Ishida, Masami & Yamazaki, Yoshiaki &Kato, Ichiro; The Realization of Dynamic Walking by the Biped Walking Robot WL-10 RD, Journal of the Robotics Society of Japan, 1985, Volume 3, Issue 4, Pages 325-336, Released on J-STAGE August 25, 2010, Online ISSN 1884-7145, Print ISSN 0289-1824,

Takanishi, Atsuo. (2018). Historical Perspective of Humanoid Robot Research in Asia. 10.1007/978-94-007-7194-9_145-1.

Tang, Zhe & Er, Meng. (2007). Humanoid 3D Gait Generation Based on Inverted Pendulum Model. 339 - 344. 10.1109/ISIC.2007.4450908.

Wang, Haitao & Tian, Zhongyuan & Hu, Wenbin & Zhao, Mingguo. (2018). Human-Like ZMP Generator and Walking Stabilizer Based on Divergent Component of Motion. 10.1109/HUMANOIDS.2018.8624926.

Waseda University WABIAN-2R, 2013; http://www.takanishi.mech.waseda.ac.jp/top/research/wabian/

Waseda University WL Robots, 2000; https://www.humanoid.waseda.ac.jp/booklet/kato_4.html

Yu, Zhangguo & Huang, Qiang & Ma, Gan & Chen, Xuechao & Zhang, Weimin & Li, Jing & Gao, Junyao. (2015). Design and Development of the Humanoid Robot BHR-5. Advances in Mechanical Engineering. 2014. 1-11. 10.1155/2014/852937.